Development of novel QbD methods for understanding manufacturing process of pharmaceutical products

Yoshihiro Hayashi

Contents

List of publications

1. Modeling of latent structure of indomethacin solid dispersion tablet using Bayesian networks. Yoshihiro Hayashi, Shingo Kikuchi, Kozo Takayama. *Drug Dev. Ind. Pharm.*, 37; 1290–1297 (2011) <presented in Chapter 1 of this dissertation>

2. Reliability evaluation of nonlinear design space in pharmaceutical product development. Yoshihiro Hayash, Shingo Kikuchi, Yoshinori Onuki, Kozo Takayama. *J. Pharm. Sci.*, 101; 333–341 (2012) <presented in Chapter 2 of this dissertation>

3. Latent structure analysis of the process variables and pharmaceutical responses of an orally disintegrating tablet. Yoshihiro Hayashi, Etsuko Oshima, Jin Maeda, Yoshinori Onuki, Yasuko Obata, Kozo Takayama. *Chem. Pharm. Bull.,* 60; 1419–1425 (2012) <presented in Chapter 3 of this dissertation>

4. Prediction of Tablet Characteristics from Residual Stress Distribution Estimated by the Finite Element Method. Yoshihiro Hayashi, Takahiro Miura, Takuya Shimada, Yoshinori Onuki, Yasuko Obata, Kozo Takayama. *J. Pharm. Sci.,* 102; 3678–3686 (2013) <presented in Chapter 4 of this dissertation>

Abbreviations

AIC; Akaike information criterion
BS; bootstrap
CI; confidence interval
CQAs; critical quality attributes
Cross-PVP ; cross povidone
CS; cornstarch
DOE; design of experiment
DPC; Drucker–Prager Cap
DS; design space
DT; disintegration time
D_{10}; dissolution rate at 10 min
D_{30}; dissolution rate at 30 min
D_{60}; dissolution rate at 60 min
d_{50}; mean size
FEM; finite element method
f_2; similarity factor
ICH; International Conference on Harmonisation
IMC; indomethacin
LAC; lactose
L-HPC; low-substituted hydroxypropylcellulose
LOOCV; leave-one-out cross-validation
MCC; microcrystalline cellulose
MDL; minimum description length
MRA; multiple linear regression analysis
ML; maximum log likelihood
PLS; partial least squares
PVP ; polyvinylpyrrolidone
Q_β; quantities of β-mannitol
QbD; quality by design
R_w; relative width
RSM; response surface method
RSM-S; response surface method incorporating thin-plate spline interpolation
S_w; specific surface area
TPS; thin-plate spline interpolation
TS; tensile strength
α_3; skewness
α_4; kurtosis

General introduction

Tablets are a very commonly and widely used dosage form for the oral administration of drugs.[1] Tablets have advantages over other dosage forms of drug delivery, such as physicochemical stability, accurate dosages and the ease of drug-release control. Moreover, tablets are convenient for patients because they are portable and easy to administer. The optimum manufacturing condition is varied by a kind and an amount of active ingredient because characteristics of active ingredient have an influence on pharmaceutical characteristics.[2] In addition, the relationships among the design variables and pharmaceutical characteristics are intricate since there are numerous factors that must be taken into account. Therefore, the expertise and experience of formulators are essential for the design of an acceptable product formulation and of a manufacturing process. However, the empirical approach requires a long development time and significant resources.

In recent years, the application of statistical methods to pharmaceutical development has been implemented, to allow International Conference on Harmonisation (ICH) Q trio guidance (Q8, Q9, and Q10).[3–5] The ICH Q8(R2) guideline announced that pharmaceutical design and development should be based on science, rather than being based on empirical knowledge only. The concept of "quality by design" (QbD) is described in the ICH Q8 recommendations, which propose that the design and development of pharmaceutical formulations and manufacturing processes should ensure the prescribed quality by understanding how these factors affect the quality of pharmaceutical products. This requires the use of a combination of chemometric treatments, including the design of experiments (DOE), the response surface method (RSM), and multivariate analyses.

DOE is a structured and organized technique to determine the factors that may influence a product or process. DOE overcomes the problems associated with one-component-at-a-time experiments that cannot clarify interactive effects between factors. DOE also helps us understand how typical fluctuations around mean input values can influence the final product.

The response surface method (RSM) is used for DOE analysis and resolving optimization problems.[6–12] However, predictions based on the quadratic polynomial method are sometimes limited, and the results obtained occasionally exhibit poor estimation. To overcome this problem, a nonlinear response surface method incorporating multivariate spline interpolation (RSM-S) was developed. The basic concept of multivariate spline interpolation involves a boundary element method.[13] Green's functions are used for minimum curvature interpolation of multidimensional data points. Prediction accuracy of RSM-S is higher than conventional techniques such as the quadratic polynomial method and multiple regression analysis in a lot of cases. In addition, this method does not require any complicated methodology such as an artificial neural network, and it has been applied to practical cases to optimize pharmaceutical formulations.

To date, various results have suggested that RSM-S is a potential tool for pharmaceutical tablet manufacturing process.[14–18] However, several difficulties are yet to be overcome regarding a non-linear technique such as RSM-S. For instance, there are no proper method of analyzing the relationships of the latent structure among the design variables and response variables, and evaluating the reliability of border on design space (DS) estimated by RSM-S. Moreover, the mechanistic understanding of pharmaceutical unit operations is limited. The purpose of this study was to overcome these problems and establish valuable tools for the pharmaceutical design under the QbD concept.

In Chapter 1, I attempted to clarify the latent structure underlying the causal factors and pharmaceutical responses of a tablet containing solid dispersion (SD) of indomethacin (IMC) using a Bayesian network (BN). In Chapter 2, a reliability of border on the DS estimated by RSM-S was evaluated using a resampling method with replacement. In Chapter 3, a multivariate statistical technique was applied to the design of an orally disintegrating tablet and to clarify the causal correlation among variables of the manufacturing process and pharmaceutical responses. In Chapter 4, the mechanical behavior of pharmaceutical powders during compaction was analyzed using the finite element method (FEM). I evaluated

differences in stress distribution between tablets composed of various formulations. Moreover, the predictive abilities of tablet characteristics of tensile strength and disintegration time on residual stress distribution were investigated.

Chapter 1

Modeling of latent structure of indomethacin solid dispersion tablet using Bayesian networks

1. Introduction

The solid dispersion (SD) system is one of the methods used to enhance the dissolution rates of drugs with limited water solubility in inert carriers. Many studies of SD carriers have been reported[19]. Polyvinylpyrrolidone (PVP) is recognized as a superior polymer for use as an SD carrier.[20–22] However, there are several disadvantages of the SD method, including manufacturing difficulties, i.e. the SD powders are generally soft and tacky with poor flowability and compressibility.[23] Therefore, the SD is rather difficult to handle when a tablet is chosen as the final product formulation.

A Bayesian network (BN) is potentially useful in formulation development. BN is a directed acyclic graphical approach that expresses the probabilistic causal relationships among attributes, in which probabilistic relationships are expressed by nodes and the links connecting the nodes.[24] BN offers many advantages over a sample of all possible observations. From the influence diagram, the dependence, independence, and/ or interdependence of variables can be determined visually as parents and offspring. In addition, not all probabilities or relationships need to be known or calculated to make a decision; adventitious relationships can essentially be ignored. I can easily determine the model structure and dependency between variables as parameters of the conditional probability distribution by using BN. Recently, BN has been used widely in various fields, including applied statistics, medicine, and bioinformatics.[25–28]

The purpose of this chapter was to clarify the latent structure underlying the causal factors and pharmaceutical responses involved in preparing indomethacin (IMC) SD tablets with high hardness and high storage stability.

2. Materials and methods

2.1. Materials

Indomethacin (IMC), a model poorly water-soluble drug, and magnesium stearate (Mg-St) were purchased from Wako Pure Chemical Industries, Ltd (Osaka, Japan). Polyvinylpyrrolidone (PVP) K30 was purchased from Sigma-Aldrich Co., Ltd (St Louis, MO, USA). Microcrystalline cellulose (MCC; Ceolus PH-101, Asahi Kasei Chemicals Co., Ltd, Tokyo, Japan), lactose (LAC; 200-mesh grade, DMV International, Veghel, the Netherlands), low-substituted hydroxypropylcellulose (L-HPC; LH-21, Shinetsu Chemical Co., Japan), and corn starch (CS; Nihon Shokuhin Kako Co., Ltd, Tokyo, Japan) were gifts from Daiichi Sankyo Co., Ltd (Tokyo, Japan).

2.2. Preparation of SDs and physical mixtures

An IMC/PVP SD was prepared using the solvent evaporation technique. Equal parts of IMC and PVP were dissolved in 95% (v/v) ethanol at 60 °C to produce a clear solution. The solvent was then removed at reduced pressure (14 mmHg) at 60 °C, using a rotary evaporator. The final residue was maintained at reduced pressure for 24 h to completely eliminate the solvent. It was then milled and the particles passed through a 250 μm sieve. These were then stored in a desiccator over silica gel to prevent their absorption of humidity. This sample was analyzed by differential scanning calorimetry (DSC; Thermo plus DSC 8230, Rigaku, Tokyo) and a powder X-ray diffractometer (XRD; RINT-1400 X-ray diffractometer, Rigaku, Tokyo), and the amorphous state of the IMC was confirmed. A physical mixture (PM) was obtained by blending IMC and PVP in a polyethylene bag.

2.3. Experiment design

An L16 (2^5) fractional factorial experimental design was used to evaluate the relative contributions of the effects of the causal factors. The IMC tablets prepared as SD or PM (X_1), the quantities of Mg-St (X_2), MCC (X_3), and L-HPC (X_4), and the compression force (X_5) were

selected as the causal factors. The 16 kinds of tablet formulations prepared are summarized in Table 1. The total mass of each tablet was adjusted to 200 mg using LAC and CS in a ratio of 7:3 (w/w).

Table 1. Test formulations composed of five causal factors based on an L16 (2^5) fractional factorial experimental design and their response variables

Rp.	Causal factors					Response variables			
	X_1	X_2 (%)	X_3 (%)	X_4 (%)	X_5 (kN)	D_{10} (%)	D_{60} (%)	TS (MPa)	f_2 (%)
1	SD	1	5	5	8	24.7±2.0	49.7±2.1	1.002±0.065	41.5±3.3
2	SD	1	5	15	12	17.6±1.1	56.7±1.9	1.337±0.069	41.6±1.0
3	SD	1	15	5	12	29.9±3.1	63.6±4.8	1.026±0.068	58.5±9.6
4	SD	1	15	15	8	36.0±4.5	59.6±1.9	1.093±0.066	51.9±1.8
5	SD	3	5	5	12	25.3±0.8	67.8±1.5	0.658±0.119	53.5±8.9
6	SD	3	5	15	8	41.6±3.5	68.0±2.4	0.447±0.031	75.3±9.6
7	SD	3	15	5	8	41.5±2.8	69.8±2.4	0.522±0.041	72.7±10.0
8	SD	3	15	15	12	19.6±1.6	66.8±4.5	0.601±0.011	47.8±3.3
9	PM	1	5	5	12	19.3±1.9	30.5±0.5	0.882±0.065	82.2±8.2
10	PM	1	5	15	8	21.4±0.4	31.4±0.5	0.844±0.043	69.6±0.9
11	PM	1	15	5	8	17.1±1.5	29.1±0.1	1.100±0.095	78.0±6.6
12	PM	1	15	15	12	18.9±1.7	30.5±0.7	1.480±0.037	76.8±2.8
13	PM	3	5	5	8	21.8±2.0	37.9±0.4	0.540±0.118	79.3±4.3
14	PM	3	5	15	12	20.4±5.8	40.9±4.3	0.770±0.063	74.7±5.0
15	PM	3	15	5	12	17.7±2.2	38.7±0.9	1.055±0.103	74.9±6.2
16	PM	3	15	15	8	21.2±3.7	39.1±0.3	1.017±0.063	70.8±7.3

X_1 is the IMC tablets prepared as solid dispersions (SD) or physical mixture (PM). X_2 is the quantities of magnesium stearate (Mg-St). X_3 is the quantities of microcrystalline cellulose (MCC). X_4 is the quantities of low-substituted hydroxypropyl (L-HPC). X_5 is the compression force. D_{10} and D_{60} are dissolution rates at 10 and 60 min, respectively. TS is tensile strength. f_2 is similarity factor.

2.4. Preparation of IMC tablets

All ingredients were dried at 75 °C for 12 h. The ingredients were accurately weighed according to the experimental formulations and all the ingredients were blended in a

polyethylene bag for 2 min. The final blend was directly compressed into round-faced tablets (200 mg, 8 mm diameter) with a tableting machine (Handtab-100, Ichihachi-Seiki Co., Ltd, Kyoto, Japan).

2.5. Dissolution test

The dissolution test was performed with a JP XV dissolution test apparatus (paddle method) using 900 mL purified water at 37 °C with stirring at 50 rpm. The samples were withdrawn and filtered after 5, 10, 15, 20, 30, 40, 50, and 60 min. The IMC concentration in the medium was measured spectrophotometrically at 320 nm with a Jasco Ubest-30 spectrophotometer (Japan Spectroscopic Co. Ltd, Tokyo, Japan). The dissolution rates of the IMC tablets at 10 min (D_{10}) and at 60 min (D_{60}), measured before and after the accelerated test, were selected as the pharmaceutical responses. The dissolution rates of three tablets of each formulation were measured.

2.6. Hardness test

The hardness of the tablet was determined with the Tablet Hardness Tester (Ogawa Seiki Co., Tokyo, Japan). Tensile strength (TS) was calculated as:

$$\mathrm{TS} = \frac{2\mathrm{F}}{\pi \mathrm{dt}} \quad (1)$$

where *F* is the maximal diametrical crushing force, and *d* and *t* are the diameter and thickness of the tablet, respectively. The TSs of three tablets of each formulation were measured.

2.7. Accelerated test

To evaluate the effects of stress conditions on the dissolution profiles and TS, the accelerated test was performed by storing the tablets at 40 °C and 75% relative humidity for

two weeks in a stability chamber (CSH-110; ESPEC Co., Osaka, Japan). The samples were then stored in a desiccator over silica gel at room temperature.

2.8. Evaluating the storage stability of IMC tablets

The similarity factor (f_2) was used to evaluate the similarity of the dissolution profiles before and after the accelerated test. f_2 is a measure of the similarity in the percentage dissolution between two curves.[29] In this study, f_2 was used as the criterion of storage stability of the dissolution profiles from 5 min to 60 min.

2.9. Analysis of variance

To evaluate the significance of the effect of causal factors and their interactions, the data obtained from the experimental design were analyzed by analysis of variance (ANOVA). The revised sum of squares (S′) obtained by subtracting the mean square of the error term from the mean square of each factor was used to estimate the contribution ratio. Contribution ratios of less than 5% were pooled as the error term.

2.10. BN model construction

The BayoNet System software, version 4.0.2 (Mathematical Systems Inc., Tokyo, Japan) was used to determine the BN structure. In this study, a greedy search strategy is applied as the K2 algorithm in the learning process of a BN. The K2 algorithm, which is a study algorithm for this type of graph structure, is the most famous score-based algorithm in Bayesian networks, and it automatically leads to the network structure from the statistical data.[30] The procedure of this search algorithm is as follows: (1) the candidates are limited that can become new nodes for each node; (2) a child node is selected, and addition of the candidate nodes are made one by one to make a graph of the network; (3) the estimated network is evaluated using statistical parameters; (4) only when the network is highly evaluated is it used as a new node; (5) when there are no more new additional node candidates

or the highest evaluation has been obtained, another child node is selected; and (6) the procedure of (1) to (5) is repeated for all child nodes. As measures of appropriateness, Akaike's information criterion (AIC), minimum description length (MDL), and maximum log likelihood (ML) were used. To construct the BN, candidates for the parent node (explanatory variable) were required. In this study, the factors were assigned as the candidates, and the responses of the tablets (D_{10}, D_{60}, and TS) were assigned as the child nodes (dependent variables). The responses of the tablets were discretized into three categories (low, medium, and high) using the K-means method on the BayoNet system.

3. Results

3.1. Responses before and after the accelerated test

Figure 1 shows the dissolution profiles for IMC from formulations Rp.2, Rp.7, Rp.11, and Rp.13, shown as typical examples. Before the accelerated test, the D_{60} values for the SD tablets were higher than those for the PM tablets, as summarized in Table 1. After the accelerated test, the initial dissolution rate was increased in the SD tablets, although that of the PM tablets had hardly changed. When analyzed by DSC and XRD, no recrystallization of IMC was seen in the SD tablets after the accelerated test (data not shown). Table 1 also shows the TS values for the test formulations before the accelerated test. The TS values for the PM tablets improved after the accelerated test, although those of the SD tablets were hardly changed (data not shown).

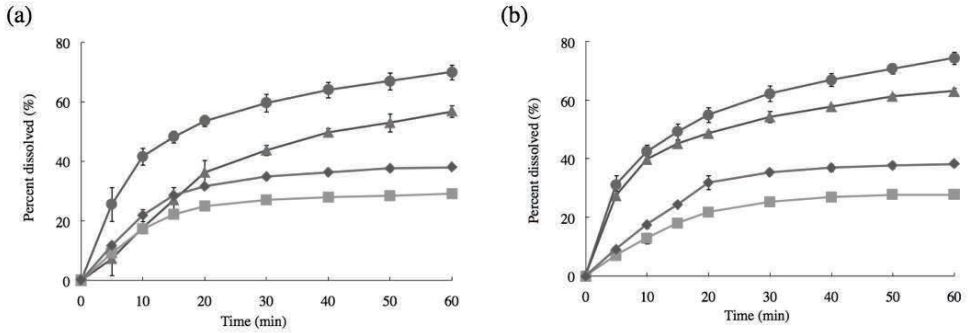

Fig. 1. Typical examples of the dissolution profiles of IMC tablets. (▲) Rp.2, (●) Rp.7, (■) Rp.11, and (◆) Rp.13 (a) before and (b) after the accelerated test.

3.2. Evaluation of causal relationships using ANOVA

To clarify the causal relationships between the formulation factors and the pharmaceutical responses, ANOVA was applied before the BN analysis. The causal factors X_1 and X_5 and the two interactions $X_1 \times X_5$ and $X_4 \times X_5$ significantly affected D_{10}, and the contributions of X_1 and X_5, in particular, were extremely high compared with those of the other factors. The contribution ratios for D_{60} indicated that more than 80% of the variance was attributable to X_1. Furthermore, X_2 strongly affected the TS values, and X_1 significantly affected the f_2 factor.

3.3. Visualization of the latent structure using BN

To visualize the latent structure between the causal factors and the responses, a BN method was applied to the data points. The optimal BN models were predicted using AIC, MDL, and ML as the judging standards (Fig. 2). The numbers of links in the BN models based on AIC, MDL, and ML were 9, 5, and 16, respectively. The BN model with MDL was the simplest and the model with ML was the most complicated. The intermediate model was obtained with AIC. These BN models were compared with the results obtained with ANOVA. Because the model based on AIC was closest to the results of ANOVA, it is likely that the AIC model appropriately demonstrates the latent structure of the tablet formulation containing IMC SD. D_{10} was affected by X_1, X_4, and X_5, D_{60} was affected by X_1 and X_4, and TS was affected by X_1, X_2, and X_3. The factor f_2 correlated predominantly with X_1.

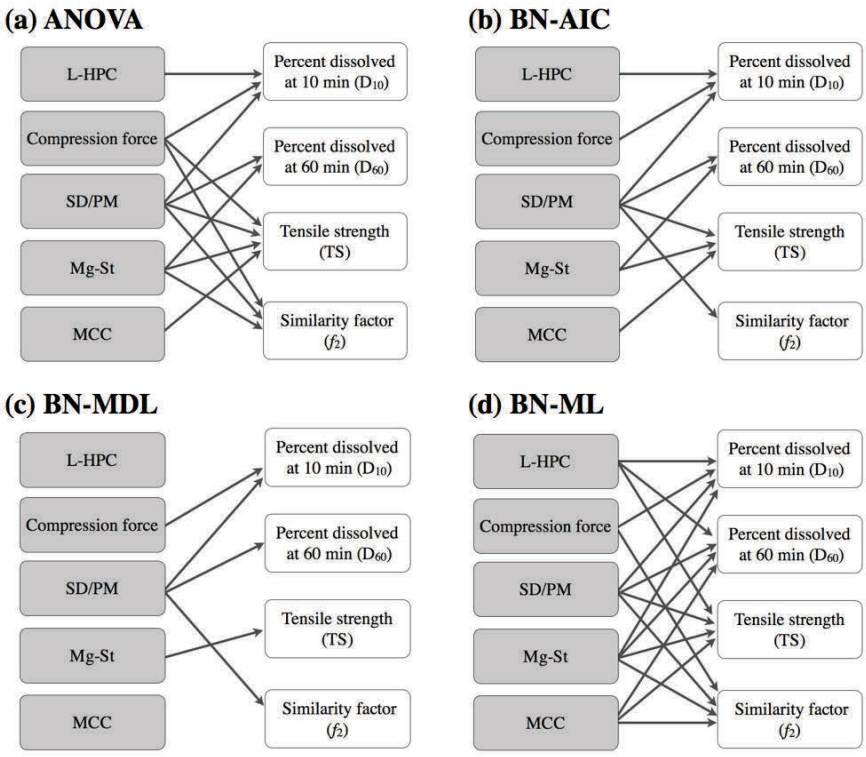

Fig. 2. Network models between causal factors and responses estimated by (a) ANOVA and (b)–(d) BN models based on three judging standards (b) Akaike's information criterion (BN-AIC), (c) minimum description length (BN-MDL), and (d) maximum log likelihood (BN-ML). The nodes correspond to the causal factors and pharmaceutical responses, respectively, and the links represent the dependencies between them.

3.4. Prediction of the responses using BN

The responses were predicted using conditional probability distributions (CPDs). As shown in Fig. 3a, the CPDs indicated whether SD or PM was crucial to the high or low values for D_{10}. The SD tablets produced with 15% L-HPC and 8 kN compression force resulted in the highest D_{10} value. In contrast, the lowest D_{10} value occurred when the tablets were made with PM and 12 kN compression force. When the tablets contained SD and 3% Mg-St, high D_{60} values were observed. In contrast, low D_{60} was predicted when the tablets were made of PM and 1% Mg-St (Fig. 3b). TS was lower when the quantity of Mg-St was high (3%). The tablets with PM, 1% Mg-St, and 15% MCC resulted in high values for TS. However, the tablets with SD and 3% Mg-St had low TS values (Fig. 3c). The SD tablets showed a tendency for low f_2, whereas the PM tablets had high f_2 (Fig. 3d). The dissolution profiles before and after the accelerated test were less similar when SD was used in the tablets.

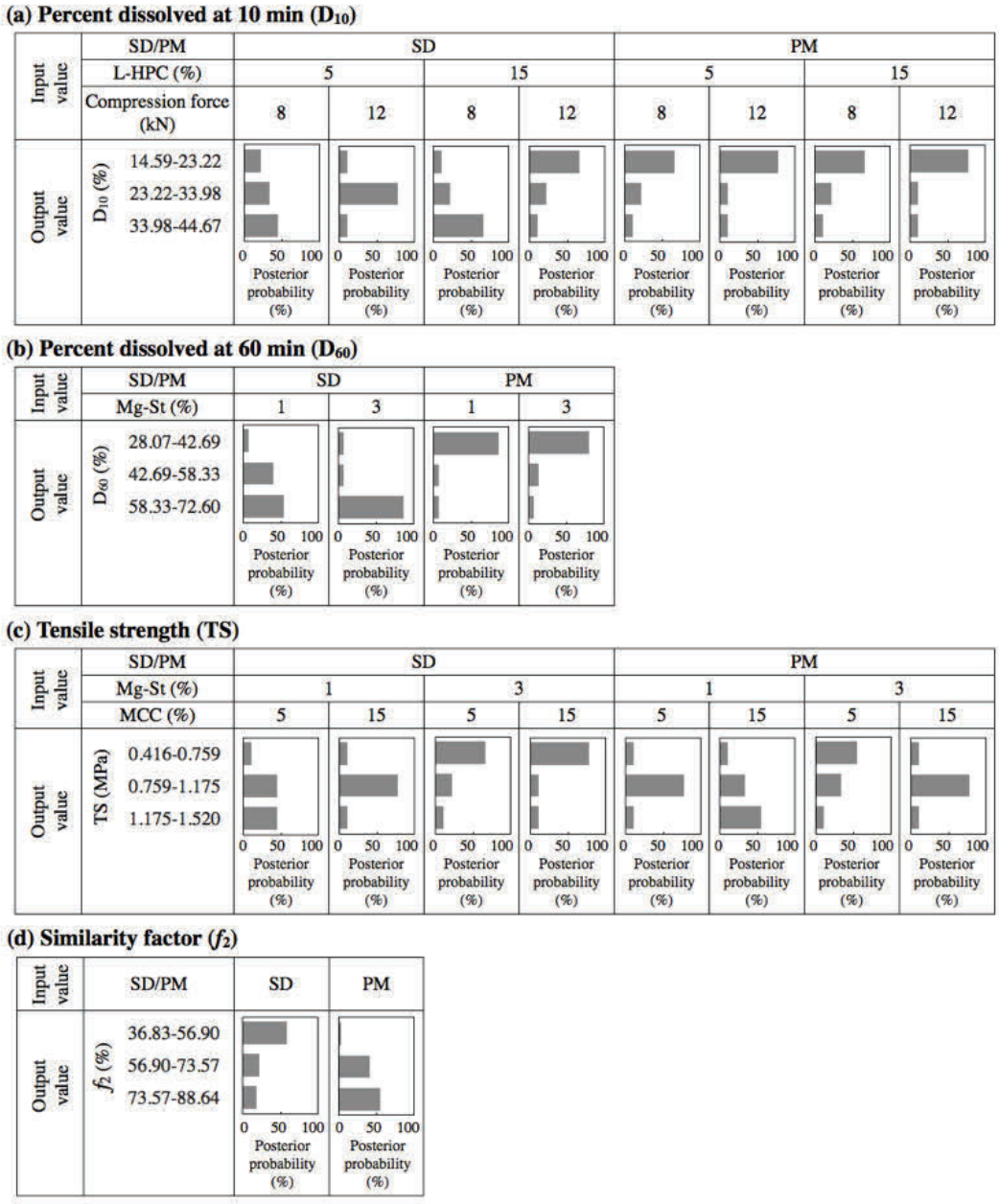

Fig. 3. Conditional probability distributions (CPDs) of the pharmaceutical responses (a) D_{10}, (b) D_{60}, (c) TS, and (d) f_2 inferred by BN. Causal factors associated with each response are set as prior probabilities. CPDs of the responses are estimated for overall combinations of the causal factors.

3.5. Prediction of causal factors using a BN model

With BN modeling, the posterior probability of the causal factors is also predicted using CPDs. To clarify the effects on D_{10} and D_{60}, the posterior probabilities of the causal factors were predicted from D_{10} and D_{60}. When the tablets had a low D_{60}, the BN model inferred a

formulation with IMC PM. When the tablets had a low D_{10} and a high D_{60}, the BN model inferred a formulation with IMC SD, high quantities of Mg-St and L-HPC, and a high compression force. Conversely, when the tablets had a high D_{10} and a high D_{60}, the BN model inferred a formulation with IMC SD, large quantities of Mg-St and L-HPC, and a low compression force. Furthermore, the tablets that had low D_{10} and high D_{60} required a much higher compression force than did the tablets with high D_{10} and high D_{60} (Fig. 4).

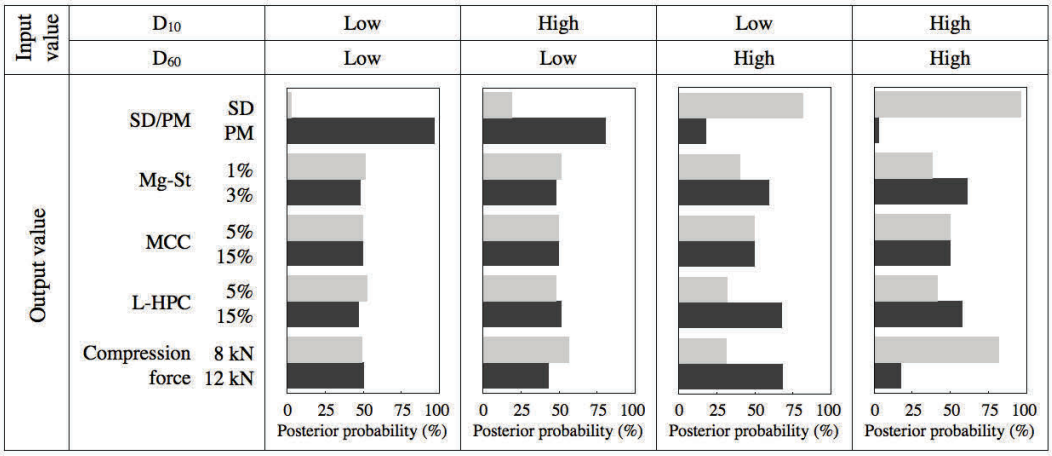

Fig. 4. Conditional probability distributions (CPDs) of causal factors inferred by BN. Dissolution properties are set as the prior probabilities. The CPDs of the causal factors are estimated for four cases: low D_{10} and low D_{60}; high D_{10} and low D_{60}; high D_{10} and low D_{60}; and high D_{10} and high D_{60}.

To predict an IMC tablet with excellent properties, i.e., high dissolution rate, high hardness, and stable storage properties, the posterior probabilities of the causal factors were predicted. IMC SD, low quantities of Mg-St and MCC, a high quantity of L-HPC, and 8 kN compression force were estimated to be the best combination of causal factors (Fig. 5).

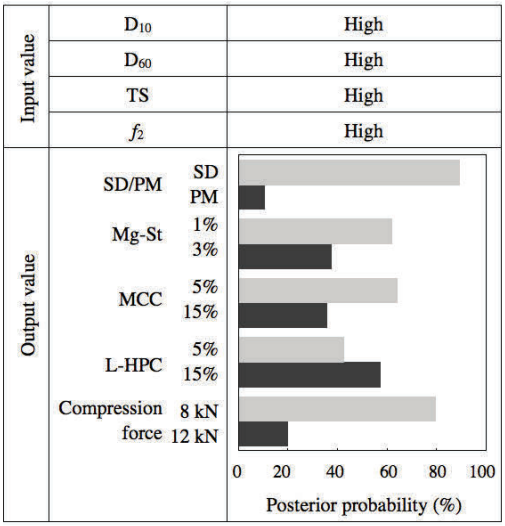

Fig. 5. Conditional probability distributions (CPDs) of causal factors inferred by BN. CPDs of the causal factors were estimated for the best combination of response variables, such as high values for D_{10}, D_{60}, TS, and f_2.

A leave-one-out cross-validation study was performed to evaluate the prediction accuracy of the BN model. The classification accuracies for D_{10}, D_{60}, TS, and f_2 were shown to be 83.3%, 83.3%, 77.1%, and 62.5%, respectively, suggesting that the BN model classified the responses into each category well.

4. Discussion

In the development of pharmaceutical formulations, the relationships between causal factors and pharmaceutical responses are often complex. It is also difficult to determine these relationships quantitatively. A BN is a graphical probabilistic model consisting of nodes as the variables and links as the dependencies among the variables. In this study, a BN model was used to clarify the relationships underlying the causal factors and responses in IMC tablet formulations.

The D_{60} values of the IMC SD tablets were higher than those of the IMC PM tablets, whereas the D_{10} values of the IMC SD tablets were not always higher than those of the IMC PM tablets before the accelerated test. This result suggests that the SD state of IMC strongly affected D_{60}, although other factors were also important in improving the initial dissolution rate. Overall, the dissolution rate was better in the tablets containing IMC SD after the accelerated test.

An L16 (2^5) fractional factorial experimental design was used to estimate the relative intensities of the influences of five causal factors on the tablet qualities. First, the data were analyzed by ANOVA. The initial dissolution rate, D_{10}, was strongly affected by X_1 (SD or PM). This suggests that the solubility of IMC and the disintegration of the tablets were higher in the IMC SD tablets than in the IMC PM tablets. Because the SD particle itself has very rapid dissolution properties, it is likely that the IMC SD tablet disintegrates easily. Therefore, the initial dissolution of the IMC SD tablets produced high values for D_{10}. The factors X_4 (L-HPC) and X_5 (compression force) were associated with D_{10} because L-HPC works as an effective disintegrant and disintegration is also affected by the compression force. Similar results have been reported in previous papers.[31–32] D_{60} was strongly affected by X_1 (SD or PM) and X_2 (Mg-St). In contrast, the TS value was affected by the factors X_1, X_2, X_3, and X_5. Among these, the effect of X_2 (Mg-St) was strongest. Mg-St reduces the interparticle binding strength, so the hardness of the tablet decreases as the quantity of Mg-St increases. More often than not, a reduction in the hardness of the tablet increases the dissolution rate.

To analyze the latent structure of the causal factors and responses in IMC tablets, BN models were constructed based on AIC, MDL, and ML as the judging criteria (Fig. 2). All models showed that X_1 (SD or PM) affected D_{10}, D_{60}, and f_2; X_2 (Mg-St) affected TS; and X_5 (compression force) affected D_{10}. Furthermore, the BN modeling results were close to the results observed with ANOVA.

BNs efficiently implement the probabilistic inference algorithm, which estimates the probability distribution of arbitrary random variables in a model.[33–34] The CPDs of the responses of the IMC tablet were predicted using the BN model based on the AIC. When the tablets were composed of IMC SD, high values for both D_{10} and D_{60} were predicted, and vice versa. The effects of MCC and Mg-St on the TS values were observed with BN modeling. The posterior probabilities of the responses for various combinations of causal factors were appropriately estimated (Fig. 3). The BN model was able to estimate not only the effects of the causal factors on each response, but also the trends in the responses produced by the formulations as CPDs. The results indicate that BN models can reveal the relationships between the causal factors and responses in IMC tablet formulations. Regardless of changes in the D_{10} value, the tablets with a low D_{60} contained IMC PM. This suggests that D_{60} was strongly affected by whether the IMC was in the SD or PM form. The BN model implied that IMC SD, large quantities of Mg-St and L-HPC, and a compression force of 8 kN, in that order, were likely to increase D_{10} and D_{60}. Because L-HPC acts as an effective disintegrant, the initial dissolution is significantly influenced by the amount of L-HPC. Moreover, the compression force used in the manufacture of the tablets differed greatly between tablets with low and high D_{10} values, suggesting that the initial dissolution of IMC was also affected by the compression force (Fig. 4).

The CPDs of the causal factors were investigated. To prepare tablets with excellent properties, low quantities of Mg-St and MCC, a large L-HPC component, and a low compression force are suggested (Fig. 5). The BN technique can be used to predict formulations with excellent pharmaceutical properties.

5. Conclusion

The latent structure underlying the causal factors and responses of IMC tablets was modeled using the BN technique. The AIC-based BN model correlated strongly with the contribution ratio estimated with ANOVA. The complex relationships between causal factors and pharmaceutical responses were successfully determined using BN modeling. Moreover, both the causal factors and responses were predicted by the BN model using CPDs. This suggests that the combination of causal factors was predicted appropriately as posterior probabilities. We conclude that the BN technique is useful for understanding the latent structure underlying tablet formulations.

Chapter 2

Reliability evaluation of the nonlinear design space in pharmaceutical product development

1. Introduction

In the previous chapter, I have applied a BN model to clarify the latent structure underlying the causal factors and pharmaceutical responses of a tablet. However, it is difficult to quantitatively predict pharmaceutical responses using BN because factors must be discretized before model construction.

In ICH Q8(R2), it is intended to provide approaches to the rational development of the design space, which is defined as the multidimensional combination and interaction of input variables and process parameters that have been demonstrated to provide quality assurance. Therefore, the design space must be established to identify the multidimensional combinations and interactions of the many causal factors that determine the quality of the target so that working within the design space is not a postapproval change.[35]

The RSM may be a powerful tool for proposing a method to set up the design space (DS). The DS is represented by the RSM resolved at the limit of a satisfactory response and is determined from the region of successful operating ranges for multiple critical quality attributes (CQAs). The overlaps of some response surface models for multiple quality attributes enable the generation of a common design space with successful operating ranges.

Using RSM-S, we can understand nonlinear relationships between causal factors and response variables, and can estimate the high-integrity design space. It is not always easy to ensure quality with a high probability when a tablet formulation or process parameter is located at the border of the design space, and it becomes necessary to clarify the credibility inside the border of the design space. However, the reliability of the nonlinear response surface estimated by RSM-S cannot be evaluated directly using conventional statistical quantities. Thus, we applied a resampling method with replacement to evaluate the reliability of the border of DS predicted by RSM-S. The resampling method, similar to a bootstrap resampling method, is a simulation technique based on the empirical distribution of the experimental samples and can be used to evaluate the reliability of the optimal solution estimated by the RSM-S.[36–38] Skewness and kurtosis were used as the statistical indices to

evaluate the normality of the distribution of the design space border determined with resampling.

The main goal of this chapter was to evaluate the reliability of the border of the nonlinear design space estimated with RSM-S using a resampling method and to set up a conservative design space considering the reliability of the border. As the model experiment, formulation optimization of indomethacin tablets was conducted.

2. Materials and methods

2.1. Materials

Indomethacin, as a model drug, and magnesium stearate (Mg-St) were purchased from Hachidai Pharmaceutical Co. Ltd. (Osaka, Japan) and Wako Pure Chemical Industries, Ltd (Osaka, Japan), respectively. Polyvinylpyrrolidone (PVP) K30 was a gift from Nippon Shokubai Co., Ltd. (Osaka, Japan). Microcrystalline cellulose (MCC; Ceolus PH-101, Asahi Kasei Chemicals Co., Ltd., Tokyo, Japan), lactose (200-mesh grade, DMV International, Veghel, the Netherlands), and cornstarch (CS; Nihon Shokuhin Kako Co., Ltd., Tokyo, Japan) were gifts from Daiichi Sankyo Co., Ltd. (Tokyo, Japan).

2.2. Preparation of IMC

All ingredients were dried at 75 °C for 12 h. The ingredients were weighed accurately according to the experimental formulations, and all ingredients were blended in a polyethylene bag for 2 min. The final blend was compressed directly into round-faced tablets (200 mg, 8 mm diameter, 12 mm radius of curvature) using a tableting machine (Handtab-100, Ichihachi-Seiki Co., Ltd., Kyoto, Japan). The compression force was about 10 kN. All formulations comprised 25 mg of Indomethacin; 161 mg of a mixture of lactose, CS, and MCC; 12 mg of PVP; and 2 mg of Mg-St.

2.3. Experimental design

Various amounts of lactose (X_1), CS (X_2), and MCC (X_3) were selected as the formulation factors. Based on the preliminary experiments, the lower and upper limits of the levels of each factor were set as follows:

$$0 \leq X_1 \leq 112.70 \text{ (mg)} \quad (2)$$

$$48.30 \leq X_2 \leq 161.00 \text{ (mg)} \quad (3)$$

$$0 \leq X_3 \leq 88.55 \text{ (mg)} \quad (4)$$

$$X_1 + X_2 + X_3 = 161.00 \text{ (mg)}. \quad (5)$$

Therefore, the feasible experimental region in the simplex-lattice design was a trapezoidal shape. The formulation factors were assigned according to an extreme vertices design, as shown in Figure 6, and nine kinds of formulations, including duplicates of the centroid, were prepared.[39]

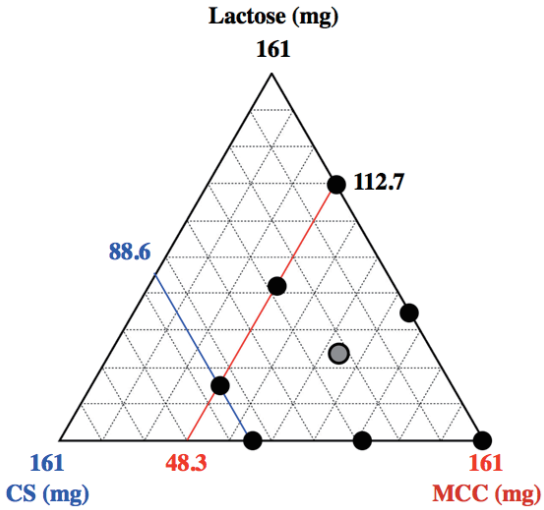

Fig. 6. Geometric representation of the experimental designs: extreme vertices design for three components. Nine formulations were assigned to the extreme vertices design in this study.

2.4. Hardness test and dissolution test

The hardness of the tablet was determined using a Tablet Hardness Tester (Ogawa Seiki Co., Tokyo, Japan). The hardness of three tablets of each formulation was measured.

The dissolution profiles of the tablets were investigated using a dissolution apparatus (JP XV Toyama Sangyo). The dissolution test apparatus was used for the dissolution test with the paddles method (JP XV) at 50 rpm using 900 mL of Japanese Pharmacopoeia XV second fluid (pH 6.8, 0.05 M H_2 KPO_4 and 0.0236 M NaOH) at 37 °C with stirring at 50 rpm. The samples were withdrawn and filtered after 3, 6, 9, 12, 15, 20, 30, and 40 min. The indomethacin concentration was measured spectrophotometrically at 320 nm with a Jasco Ubest-30 spectrophotometer (Japan Spectroscopic Co. Ltd., Tokyo, Japan). The dissolution rates of the indomethacin tablets at 30 min (D_{30}), measured before and after the accelerated

test, were selected as the pharmaceutical responses. The dissolution rates of three tablets of each formulation were measured.

2.5. Accelerated test

To evaluate the effects of stress conditions on hardness and the dissolution profiles, the accelerated test was performed by storing the tablets at 40 °C and 75% relative humidity for 4 weeks in a stability chamber (CSH-110; ESPEC Co., Osaka, Japan). The samples were then stored in a desiccator over silica gel at room temperature.

2.6. Setup of design space and reliability assessment of the design space border using the RSM-S and resampling technique

We used the resampling technique with replacement to evaluate the reliability of the design space border (Fig. 7). First, the design space was estimated based on the RSM-S using a data set obtained with an extreme vertices design. The resampling method was then applied to evaluate the reliability of the design space. The number of resamplings with replacement was fixed at 500. From the distribution of the resampling border of the design space, 95% confidence intervals (CIs) for the border of the original design space were calculated. When a lack in one or more formulation was found in the process of resampling, the relevant resampling sets were deleted from the analysis as “data set with a lack”. That is, the resampling set was arranged to include one or more data points for every formulation. This process is shown in Figure 7.

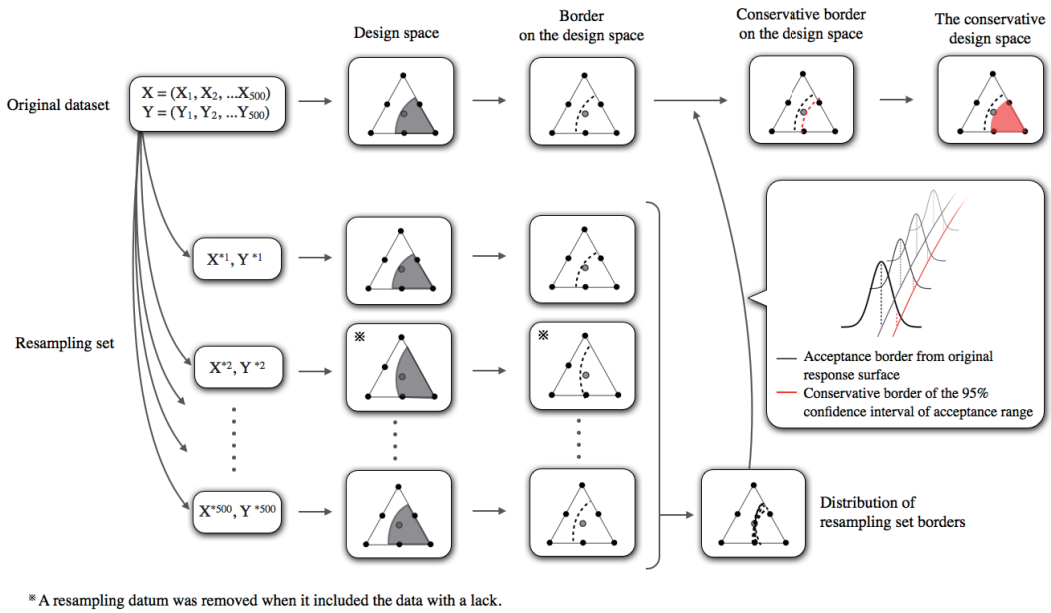

Fig. 7. Resampling process for evaluating the reliability of the border of the design space estimated by RSM-S.

Skewness (α_3) and kurtosis (α_4), indices of the normality of the histograms of the resampling borders of the design space, were calculated as:

$$\alpha_3 = \frac{n}{(n-1)(n-2)} \cdot \sum \left(\frac{x_i - \bar{x}}{s} \right)^3 \tag{6}$$

$$\alpha_4 = \left\{ \frac{n(n+1)}{(n-1)(n-2)(n-3)} \cdot \sum \left(\frac{x_i - \bar{x}}{s} \right)^4 \right\} - \frac{3(n-1)^2}{(n-2)(n-3)} \tag{7}$$

where n is the number of the resampling borders of the design space (x_i), $\bar{x}$ is the mean of x_i, and s is the sample standard deviation. When the indices α_3 and α_4 are close to 0, the histograms of the resampling border of the design space are close to a normal distribution.

2.7. Computer programs

RSM-S was performed using dataNESIA® version 3.2 (Yamatake Corp., Fujisawa, Japan). Resampling method with replacement was applied with dataNESIA® version 3.2 (Yamatake Corp., Fujisawa, Japan) and Microsoft Excel® for Windows 2007, and the macroprograms

were written by the authors with Visual Basic version 6.5 (Microsoft Corp., Tokyo, Japan). The multiple linear regression analysis was performed using Microsoft Excel® for Windows 2007.

3. Results

3.1. Prediction of the response variables using RSM-S

The hardness and D_{30} before and after the accelerated test were displayed using response surfaces, which were estimated by the RSM-S based on the original data set. The accuracy of each response surface was evaluated by leave-one-out cross-validation (LOOCV), which produced correlation coefficients ranging from 0.96 to 0.99. The response surfaces are shown in Figure 8. As shown by the response surface (Fig. 8a), hardness increased as the amount of CS decreased. A much higher hardness value was observed for tablets containing a low and high amount of CS and MCC, respectively. The tablet with a large amount of MCC had a low D_{30}, and the others had a high D_{30} before the accelerated test (Fig. 8c). The response surfaces for hardness and D_{30} were significantly different after the accelerated test compared with before the accelerated test. After the accelerated test, the hardness tended to increase and D_{30} to decrease (Fig. 8b and d). In particular, D_{30} changed markedly when the quantity of CS was 5% to 25% after the accelerated test.

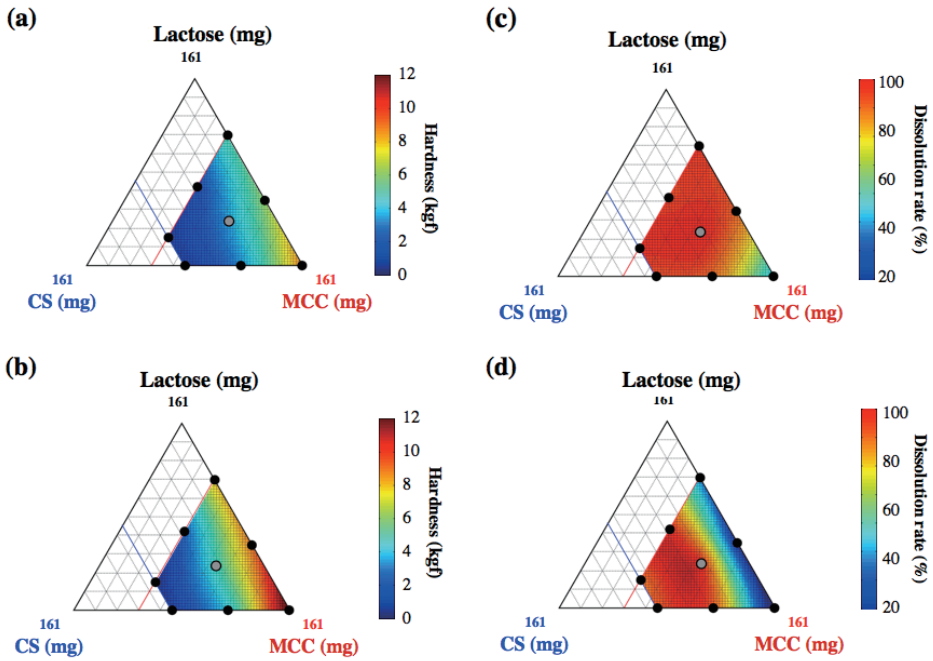

Fig. 8. Response surfaces of the indomethacin tablets estimated by RSM-S as a function of the amounts of lactose, cornstarch (CS), and microcrystalline cellulose (MCC). (a) and (b) indicate hardness before and after the accelerated test, respectively. (c) and (d) indicate the dissolution rate 30 min before and after the accelerated test, respectively.

3.2. Setup of the design space for formulation of IMC tablets using RSM-S

The nonlinear design spaces were defined as >3 kgf hardness and >70% dissolution 30 min before and after the accelerated test. Because the hardness tended to increase after the accelerated test, the criterion measure of hardness was defined as >3 kgf before the accelerated test. By contrast, because D_{30} tended to decrease after the accelerated test, an acceptable range of dissolution, defined as D_{30} >70%, was desired after the accelerated test.

3.3. Histograms of the design space border

The reliability of the design space border estimated by RSM-S was evaluated using the resampling method. Histograms of 500 resampling borders of the design space for each response are shown in Figure 9. When the resampling data included data with a lack, an outlier was observed and the data distribution deviated from normal, as shown in Figure 9a and c. However, the outliner was diminished when the data with a lack was removed from the analysis, as shown in Fig.9b and d. Kurtosis and skewness were estimated as the statistical indices to evaluate the normality of the distribution of the design space border determined with resampling method. Histogram of design space border as a function of the amount of lactose with a step size of 2.32 mg was evaluated and each value was shown as a histograms. In each case, both kurtosis and skewness deviated somewhat from 0. The normality of the histograms of the border of the design space for each response was tested using the Jarque–Bera hypothesis test. The percentages of histograms of hardness and D_{30} judged to be distributed normally were 44.6% and 22.0%, respectively.

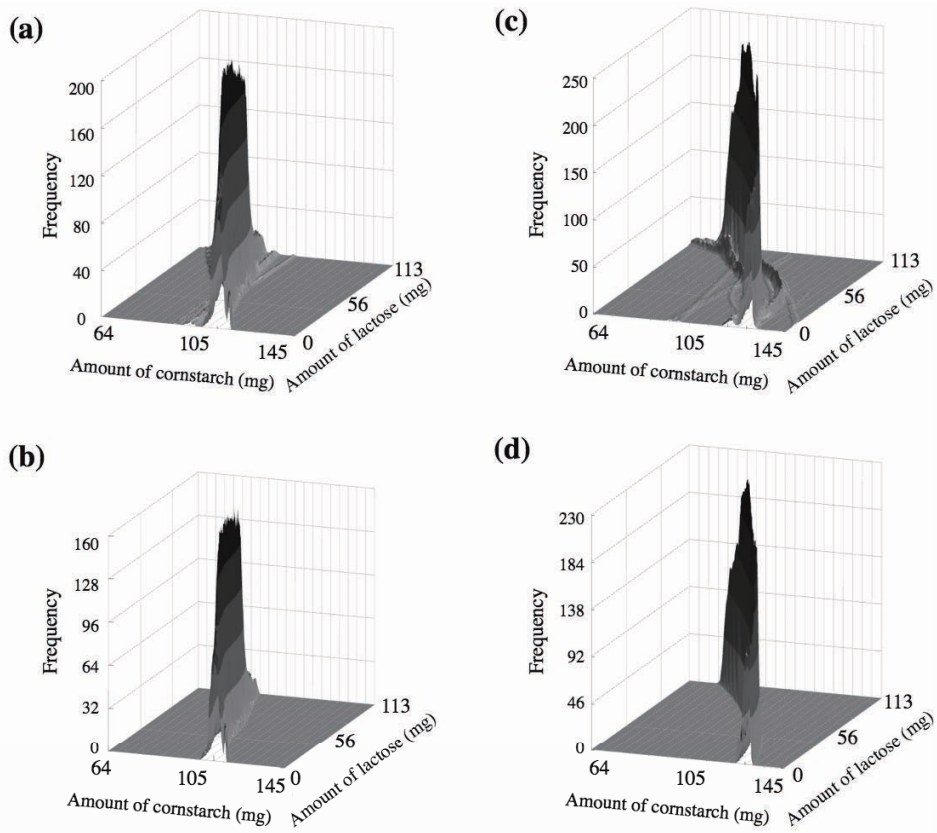

Fig. 9. Histograms of the borders of the design space estimated by the resampling set. Resampling was repeated 500 times. When the resampling set includes a lack of one or more formulations, as shown in Figure 6, the relevant set was deleted from the analysis. After this tuning of the resampling data, histograms of the border of the design space for hardness and dissolution rate at 30 min were made using 353 and 339 data sets, respectively: (a) hardness and (b) dissolution rate at 30 min.

3.4. Setup of the conservative design space

The 95% CIs of the border of the design space were estimated based on the percentile technique as a nonparametric approach. The results are shown in Figure 10a and b. The conservative and optimistic borders were defined as the 95% CIs of the acceptance ranges of the hardness and D_{30} values. The reliability of the border decreased with departures from the center, and the reliability of hardness was lower in the neighborhood of the center than that of D_{30}. Two design spaces were superimposed, and a common conservative design space was defined as the successful formulation range (Fig. 11).

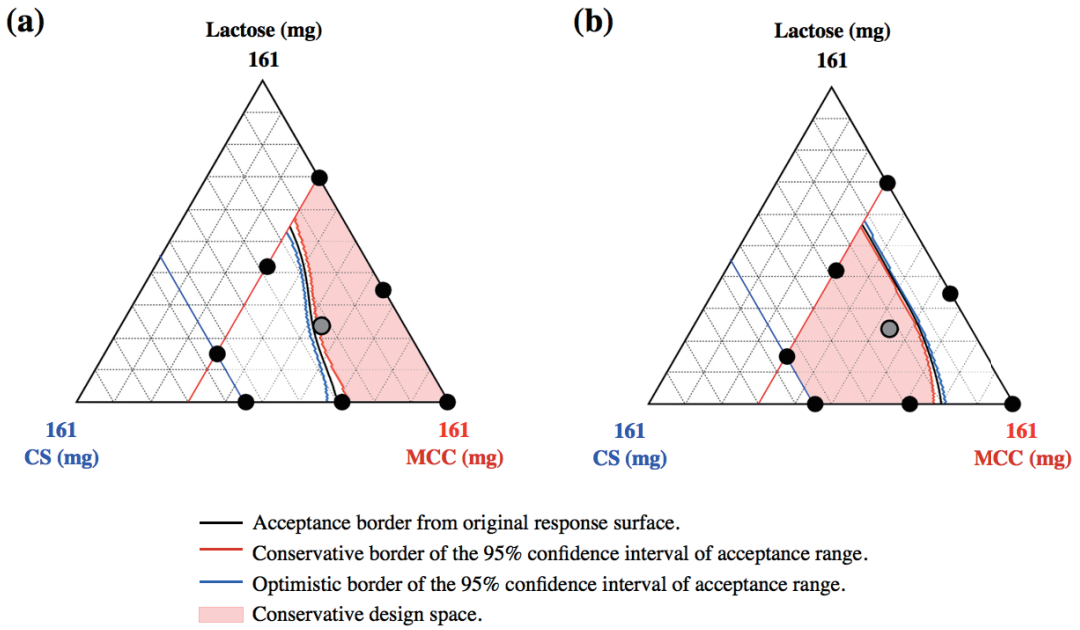

Fig. 10. Design space and 95% CIs of the design space border. (a) Hardness >3 kgf and (b) dissolution rate >70% at 30 min.

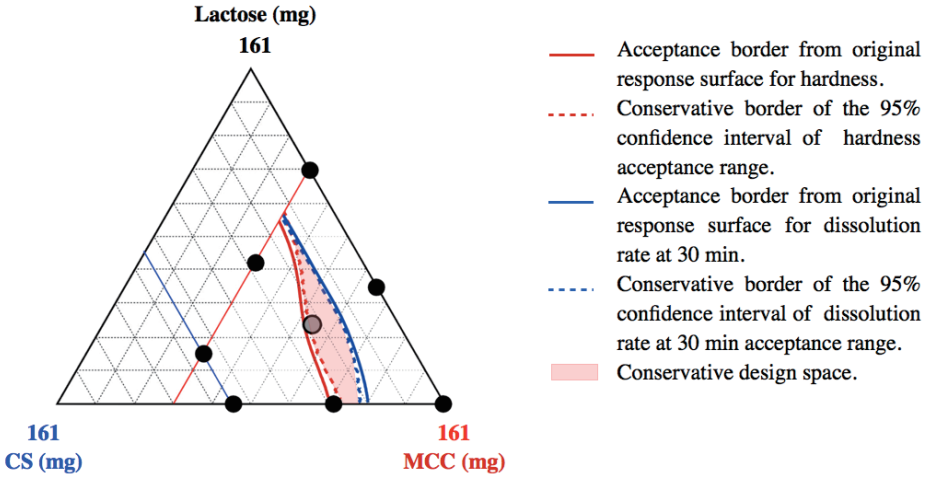

Fig. 11. Conservative design space comprising superimposed individual design spaces for hardness and dissolution rate at 30 min for the relevant 95% CIs.

3.5. Mathematization of the conservative design space

A polynomial approximation technique was applied for mathematization of the border of the nonlinear design space and produced correlation coefficients > 0.99. The conservative design space was expressed as the region implemented simultaneously in the following four mathematical formulas.

$$y > -3.118 \times 10^{-5}x^3 + 0.0059x^2 - 1.0295x + 118.21 \quad (8)$$

$$y < 1.261 \times 10^{-5}x^3 - 0.0046x^2 - 0.5556x + 125.82 \quad (9)$$

$$x, y, z > 0 \quad (10)$$

$$x + y + z = 161 \text{ (mg)} \quad (11)$$

where x, y, and z are the quantities of lactose, MCC, and CS, respectively.

4. Discussion

In this study, tablets comprising mainly lactose, CS, and MCC were prepared. Lactose, CS, and MCC were chosen as the filler, disintegrating agent, and binding agent, respectively. The response variables such as hardness and D_{30} were predicted accurately using RSM-S, as shown clearly in the results of the LOOCV. Multiple regression analysis was also performed and the coefficient of determination which was adjusted with degrees of freedom (R^{**2}), an indicator of the fit of each linear regression equation, was estimated. R^{**2} for hardness was approximately 0.90 before and after accelerated test, resulting in relatively high value, but it was worse than that of RSM-S. R^{**2} for D_{30} was approximately 0.66 before and after accelerated test, resulting in poor estimations, better result was observed with RSM-S.

To consider hardness, dissolution property, and stability, the design space was defined as the tablets whose hardness and dissolution rate at 30 min were >3 kgf and 70%, respectively, before or after the accelerated test. The shape of either border of the design space changed with the quantity of CS. This result suggests that a change in the response induced by the change in the CS amount would not be compensated by increasing the amount of lactose and MCC. By contrast, the acceptance range of the amount of lactose was larger, suggesting that changes attributed to the amount of lactose can be substituted by changes in the amounts of CS and MCC.

Five hundred borders of the design space were generated using the resampling method with replacement. Most of the histograms before omitting the data set with a lack had a far from normal distribution (Fig. 9a and c), and some showed several peaks. By deleting the data with a lack from the resampling set, the shape of the response surfaces estimated by the resampling set would be fractured considerably from the original surface.[40] For this reason, resampling sets with a lack of one or more formulations were removed. After this tuning process, about 30% of the resampling data sets were deleted and about 70% remained; the remaining data sets were used to evaluate the border of the design space. Moreover, the outliers disappeared and most of the histograms after clustering seemed to be symmetrical in appearance. To estimate the stability of the reliability of the optimal formulation using the

RSM-S and bootstrap resampling method, a resampling frequency of >50 was sufficient.[16] Therefore, 350 resampling sets corresponding to 70% of the total resampling data should be sufficient to estimate the reliability of the border of the design space.

To evaluate the robustness of the border of the design space, histograms of the border were calculated using the resampling technique. The resampling technique is a statistical interval analysis that uses a Monte Carlo simulation. To provide the special benefit of the central limit theorem, the shape of the histogram constructed from the arithmetic means of the resampling samples follows a normal distribution. It is not possible to hypothesize the central limit theorem to the border of the design space derived from RSM-S, so the distribution of the resampling design space border must be evaluated. Kurtosis and skewness were used as indices of normality to evaluate the shape of the distribution of the resampling border of the design space (Fig. 12).

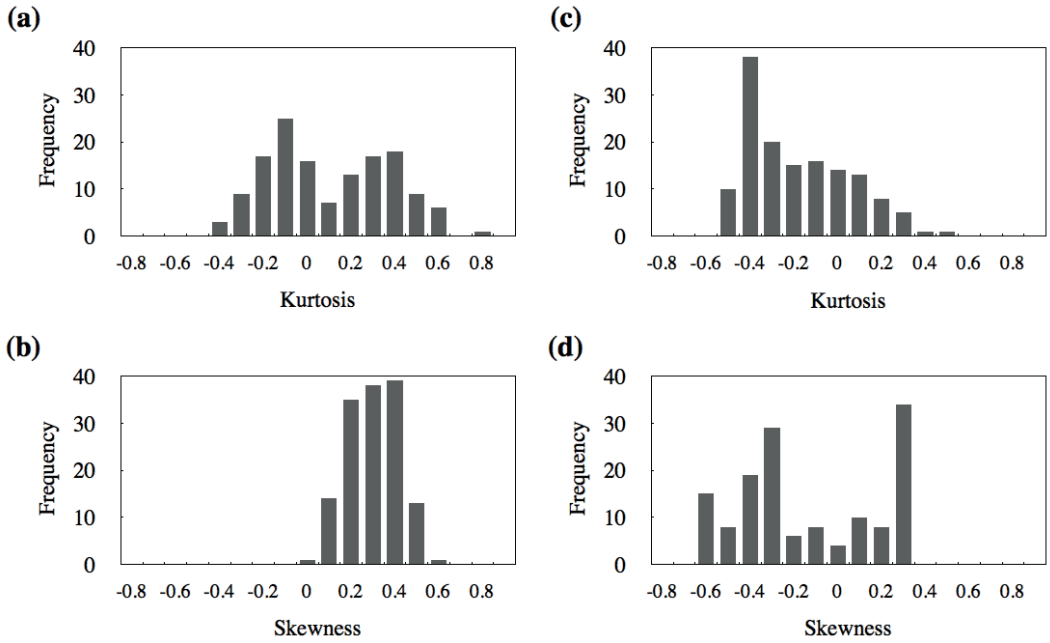

Fig. 12. Histograms for kurtosis and skewness for the design space border: (a) and (b) indicate kurtosis and skewness of the design space border of hardness, respectively. (c) and (d) indicate kurtosis and skewness of design space border of the dissolution rate at 30 min, respectively.

Skewness for hardness was expressed mainly as positive values, and both skewness and kurtosis for D30 were negative values. This result suggests that the histograms of the border of the design space for hardness had an elongated tail and more data in the right tail than does a normal distribution. By contrast, the histogram of the border of the design space for D30 had an elongated tail at the left, more data in the right tail, and a sharper distribution than does a normal distribution. The Jarque–Bera test is a goodness-of-fit test of the deviation of the departure from normality based on skewness and kurtosis. In our analysis, six of 10 borders were judged to have a nonnormal distribution. When the shape of the histogram is skewed significantly, the nonparametric CI of the border is more appropriate for estimating the reliability compared with the parametric approach.[41] The percentile method is a nonparametric method for inferring CIs.[42–44] Consequently, we employed the percentile method as a nonparametric technique.

The reliability of the border of the design space decreased when approaching the edge of the experiment design. The conservative design space in Figure 11 allows robust range formulations of sufficient hardness and dissolution rate relevant to the 95% CIs. This is the first study to show that the conservative border of the nonlinear design space can be defined clearly as a third-order polynomial function of the amounts of excipients such as lactose, CS, and MCC.

5. Conclusion

A resampling method with replacement was applied to evaluating the reliability of the border of the design space estimated by RSM-S. The accuracy of the response surfaces was elucidated sufficiently, with high correlation coefficients produced in the LOOCV. However, the shape of the distribution of the border of the design space generated by the resampling method with replacement differed from a normal distribution, and the CI of the border was estimated using a nonparametric percentile technique. The conservative border of the design space relevant to the 95% CI was defined clearly as a third-order polynomial function of the amounts of excipients such a lactose, CS, and MCC. This RSM-S and resampling method would be a useful tool for estimating the reliability of the border of the nonlinear design space.

Chapter 3

Latent structure analysis of the process variables and pharmaceutical responses of an orally disintegrating tablet

1. Introduction

In previous Chapter 1 and 2, I demonstrated that BN and RSM-S were potential tool for clarifying the relationships between design variables and pharmaceutical responses.

A key goal of QbD is to identify the most important critical quality attributes (CQAs) and to understand their relationships with the product performance.[45–46] According to the ICH Q8(R2), a CQA is a physical, chemical, biological, or microbiological property or characteristic that should be within an appropriate limit, range, or distribution to ensure the desired product quality. CQAs are generally associated with the drug substance, excipients, intermediates in-process materials, or the drug product. A linkage among the causal factors, CQAs and pharmaceutical responses should enable identification and understanding of the causal factors and their impact on the CQAs

Since various unit processes are continued in pharmaceutical manufacturing process, intermediates in process have an influence on pharmaceutical characteristics. The intermediates of characteristics such as powder and granule could be CQAs. The intermediates in process materials rather than design variables were chosen as the causal factors for the response variables in order to avoid scale-gap and equipment-gap.[47] However, the relationships among the variables, intermediates in-process materials, and pharmaceutical characteristics are intricate.

In recent years, orally disintegrating tablets (ODTs) have become popular worldwide. ODTs are preferred by an increasing number of patients, especially children and the elderly, but also adults who like to have their medication readily available at any time. Various compositions and manufacturing methods of orally disintegrating or dissolving tablets have been reported.[48–50] However, ODTs have several disadvantages: they are generally brittle and a special apparatus is needed for their manufacture. Therefore, ODTs are difficult to prepare in their final dosage form.

In this chapter, I optimized the process parameters using RSM-S and determined the granule properties that are closely associated with process variables and responses of ODTs. I applied a BN to analyze the causal correlations among variables of the manufacturing process,

granules, and tablet properties. A BN was used to construct a probabilistic graphical model of the latent structure of ODTs and to reveal the latent structure in the manufacture of these tablets.

2. Materials and methods

2.1. Materials

Indomethacin (IMC), which was used as a model drug and magnesium stearate (Mg-St) were purchased from Hachidai Pharmaceutical Company, Ltd (Osaka, Japan) and Wako Pure Chemical Industries, Ltd (Osaka, Japan), respectively. The δ form of mannitol (Parteck® Delta M) was purchased from Merck KGaA (Darmstadt, Germany). Microcrystalline cellulose (MCC; Ceolus PH-101, Asahi Kasei Chemicals Co., Ltd, Tokyo, Japan) was gifts from Daiichi Sankyo Co., Ltd (Tokyo, Japan). Cross povidone (Cross-PVP; Polyplasdone® XL, ISP Co., Ltd, N.J., USA) was a gift from Nippon Shokubai Company, Ltd (Osaka, Japan).

2.2. Preparation of ODTs

Process conditions were fixed according to the flow chart presented in Figure 13. The ingredients were accurately weighed according to the experimental formulations and all ingredients, with the exception of Mg-St, were blended using a mixer (KM4005, De'Longhi, Italy) for 1 min. Distilled water was added as a granulation liquid and the mixture was kneaded (impeller speed, 470 rpm; processing time, 1–9 min). After the granulation process, the granules were sieved through a 5.8 mm mesh. The granules were dried at 75°C for 30 min and sieved through a 850 μm mesh. Mg-St was added to the granules and the mixture was blended in a polyethylene bag for 1 min. The final blend was compressed into round-faced tablets (200 mg, 8 mm in diameter, with a 12 mm radius of curvature) using a tableting machine (Handtab-100, Ichihashi-Seiki Co., Ltd, Kyoto, Japan). All the formulations were composed of 25 mg of IMC, 145 mg of δ-mannitol, 20 mg of Cross-PVP, and 10 mg of MCC.

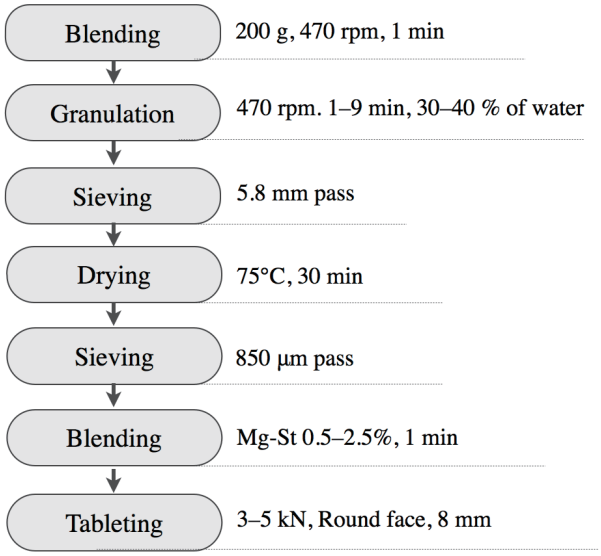

Fig. 13. Flow chart of the granulation process.

2.3. Experimental design

To develop systematic model formulations, 27 kinds of tablets containing indomethacin, δ-mannitol, Cross-PVP, MCC, and Mg-St were prepared according to a Box–Behnken design (Table 2). Water amount (X_1), kneading time (X_2), compression force (X_3), and amount of Mg-St (X_4) were selected as the design variables.

Table 2. Box–Behnken experimental design of four process parameters and response variables.

Rp.	Design variables				Response variables	
	X_1 (%)	X_2 (min)	X_3 (kN)	X_4 (%)	TS (MPa)	DT (s)
1	30	1	4	1.5	0.85±0.01	9.24±0.06
2	30	9	4	1.5	1.12±0.03	13.65±0.11
3	40	1	4	1.5	1.00±0.08	13.76±0.16
4	40	9	4	1.5	1.28±0.04	15.56±0.15
5	35	5	3	0.5	0.74±0.00	13.69±0.30
6	35	5	3	2.5	0.81±0.02	11.33±0.15
7	35	5	5	0.5	1.42±0.03	14.82±0.08
8	35	5	5	2.5	1.51±0.08	18.07±0.26
9	30	5	4	0.5	0.99±0.04	11.27±0.20
10	30	5	4	2.5	1.10±0.05	12.22±0.20
11	40	5	4	0.5	1.20±0.07	14.16±0.16
12	40	5	4	2.5	1.33±0.06	15.80±0.17
13	35	1	3	1.5	0.68±0.00	8.85±0.11
14	35	1	5	1.5	1.17±0.06	12.14±0.38
15	35	9	3	1.5	0.74±0.03	11.53±0.23
16	35	9	5	1.5	1.47±0.09	15.31±0.22
17	30	5	3	1.5	0.75±0.00	9.49±0.25
18	30	5	5	1.5	1.36±0.05	14.72±0.20
19	40	5	3	1.5	0.94±0.01	12.75±0.25
20	40	5	5	1.5	1.65±0.06	18.84±0.19
21	35	1	4	0.5	0.79±0.05	9.55±0.25
22	35	1	4	2.5	0.91±0.03	11.74±0.25
23	35	9	4	0.5	1.08±0.02	13.09±0.12
24	35	9	4	2.5	1.17±0.02	13.31±0.08
25	35	5	4	1.5	1.16±0.05	12.63±0.21
26	35	5	4	1.5	1.17±0.05	12.50±0.23
27	35	5	4	1.5	1.13±0.02	12.71±0.20

X_1 is water amount. X_2 is kneading time. X_3 is compression force. X_4 is amount of Mg-St. TS is tensile strength. DT is disintegration time. The value of TS and DT represent the mean ± S.D. for three determinations.

2.4. Evaluation of tablet properties

The hardness of the tablets was determined using a tablet hardness tester (Ogawa Seiki Co., Tokyo, Japan). Tensile strength (TS) was calculated using Eq. (1). The TS of three tablets of each formulation were measured. The disintegration test was performed according to the JP16 disintegration test for tablets using a disintegration tester (NT-20H; Toyama Sangyo Co., Ltd, Osaka, Japan) and water (as a solvent) at 37°C. Disintegration time (DT) was defined as the interval required for the complete disappearance of a tablet or its particles from the tester net. DT was measured for three tablets of each formulation. The dissolution test was performed according to the JP16 dissolution test no. 2 (the paddle method) at 100 rpm (NTR-6100A, Toyama Sangyo Co., Ltd, Osaka, Japan). The dissolution medium used was 900 mL of mixture of 1 volume of 0.05 M phosphate buffer (pH 7.2) and 4 volumes of distilled water at 37±0.5°C. The samples were collected and filtered after 5, 10, 15, 20, 25, 30, 40, and 50 min. The concentration of indomethacin was measured spectrophotometrically at 320 nm using a Jasco Ubest-30 spectrophotometer (Japan Spectroscopic Company, Ltd., Tokyo, Japan). The dissolution rates of three tablets of each formulation were measured.

2.5. Physicochemical properties of granules

Quantities of β-mannitol (Q_β), specific surface area (S_w), and mean size (d_{50}) and relative width ($R_w = (d_{10} - d_{10})/d_{50}$) of particles were measured. The Q_β of granules was determined via a combination technique using a X-ray powder diffractometer (XRD; RINT-1400 X-ray diffractometer, Rigaku, Tokyo, Japan) and a partial least squares (PLS) regression analysis.[51] These measurements were carried out at 40 kV, 40 mA with a CuKα source between 5° and 30° 2θ with a scan speed of 2.0°/min in the step scan mode.

The S_w of the granules was measured using the single-point BET method (Macsorb HM model-1201, Mountech, Tokyo, Japan). Before measurement, about 1 g of each sample was weighed in a sample tube and was then degassed for 30 min at a temperature of 60 °C using

nitrogen as the purge gas. Subsequently, the specific surface area of the granules was measured using nitrogen adsorption.

The d_{50} and R_w of granules were determined based on the distribution of particle sizes, which was measured using a sieving machine (Robot Shifter RPS-105, Seisin Enterprise, Tokyo, Japan) using the following sieves: 75, 106, 150, 212, 300, 500 and 800 μm. Samples of 10 g were passed through the sieves and stirred during a predefined time of 3 min. Finally, the powder fraction held in each sieve was weighed.

2.6. Computer programs

The nonlinear RSM was performed using dataNESIA® version 3.2 (Yamatake Corporation, Fujisawa, Japan). Multiple linear regression analysis was performed using Microsoft Excel® for Windows 2007 (Microsoft Corporation, Redmond, WA). A chemometric analysis for XRD data was performed using the PLS program associated with the Unscrambler 9.0 software (Camo Technologies, Woodbridge, NJ). The BayoNet System software, version 5.0. (Mathematical Systems Inc., Tokyo, Japan) was used to construct the probabilistic graphical model among the variables manufacturing process, granules, and tablet properties and to estimate conditional independencies.

3. Results

3.1. Prediction of the responses of tablets using RSM-S

TS and DT were measured as tablet properties. The response surfaces for each tablet property were estimated using RSM-S based on the original data set. The accuracy of the response surfaces was evaluated via leave-one-out cross-validation (LOOCV), which revealed that the correlation coefficients for TS and DT were sufficiently high (0.977 and 0.979, respectively). The response surfaces of the tablet properties are shown in Figure 14. The TS increased as the water amount (X_1), kneading time (X_2), and compression force (X_3) increased. The amount of Mg-St (X_4) had a negligible effect on TS. The DT decreased as X_1, X_2, X_3, and X_4 decreased. Formulations Rp.13 and Rp.20 showed the lowest and highest value of DT in all formulations tested, respectively. Therefore, the dissolution test was performed in the limited way to formulations Rp.13 and Rp.20. The dissolution rate at 5 min for IMC from formulations Rp.13 and Rp.20 was 93.1±1.7% and 92.1±2.6%, respectively. No significant difference was observed between Rp.13 and Rp.20.

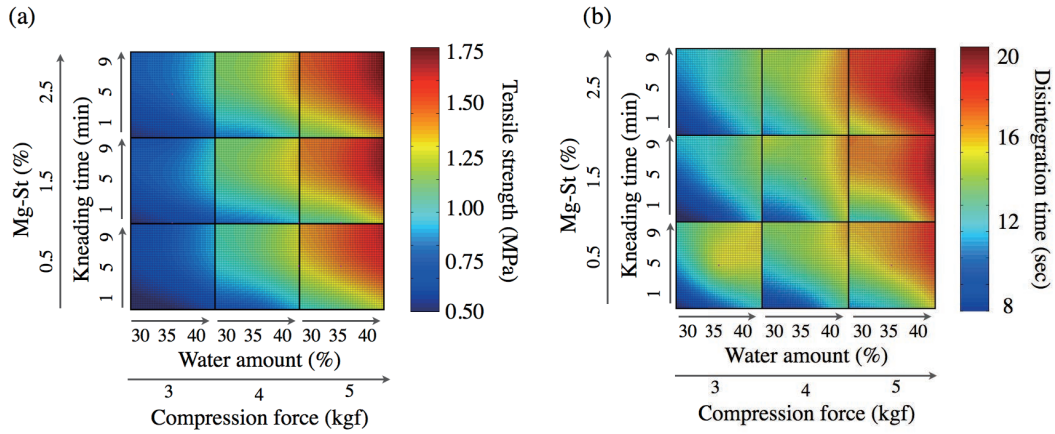

Fig. 14. Response surfaces of orally disintegrating tablets estimated using RSM-S based on water amount, kneading time, compression force, and quantity of Mg-St. Panels (a) and (b) indicate tensile strength and disintegrating time, respectively.

3.2. Optimization of process variables using RSM-S

The process variables of tablets were optimized using RSM-S based on the original data set. The optimization problem was formulated to maximize TS and to minimize DT with an

even weight within the range of experimental space. Results of the simultaneous optimum analysis are given in Table 3. The water amount (X_1) = 30.57%, kneading time (X_2) = 3.16 min, compression force (X_3) = 4.04 kN, and the amount of Mg-St (X_4) = 1.45% were estimated as the optimal process variables. The following were estimated as the optimal response variables: TS = 0.98 MPa and DT = 10.72 s. Table 3 also shows the TS and DT of the optimal process variables. The TS and DT values predicted by RSM-S coincided well with the experimental values.

Table 3. Predicted and experimental values of response variables of optimal process variables based on the RSM-S.

	Predicted	Experimental
Water amount (%)	30.57	–
Kneading time (min)	3.16	–
Compression force (kN)	4.04	–
Mg-St (%)	1.45	–
Tensile strength (MPa)	0.98	1.01±0.03
Disintegration time (s)	10.72	10.80±0.40

3.3. Prediction of granule properties using RSM-S

Q_{β}, S_w, d_{50}, and R_w were measured as granule properties. The response surfaces for each granule property were estimated using RSM-S based on the original data set. The accuracy of the response surfaces was evaluated by LOOCV, which revealed that the correlation coefficients for Q_{β}, S_w, d_{50}, and R_w were sufficiently high (0.935, 0.929, 0.899, and 0.885, respectively). The analysis of response surfaces showed that the Q_{β} and granules increased with increasing kneading time (X_2); however, water amount (X_1) had only a small effect on Q_{β}. S_w increased with increasing water amount (X_1) and kneading time (X_2). d_{50} was highest for high water amounts (X_1) and short kneading times (X_2). In contrast, R_w was highest for small water amounts (X_1) and long kneading times (X_2) (Figure 15).

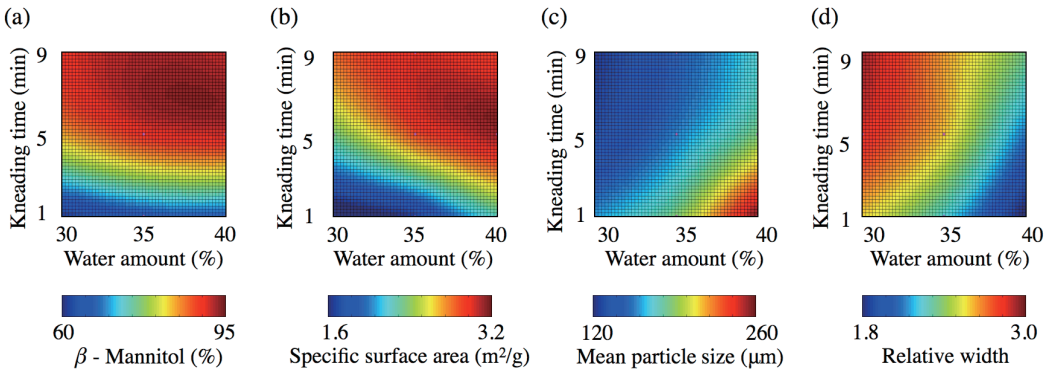

Fig. 15. Response surfaces of granule properties estimated using RSM-S based on water amount and kneading time. (a) Amount of β-mannitol, (b) specific surface area, (c) mean particle size, and (d) relative width.

3.4. Estimation of a quantitative latent structure model using a Bayesian network

An analysis of the causal relationships among process variables and granule and tablet properties was used to estimate the latent structure model using a BN. All variables were discretized to three levels for the inference of the conditional probability distribution. The optimal BN models were predicted using Akaike's information criterion (AIC), the K2 algorithm, and minimum description length (MDL) as the judging standards. The accuracy, precision, recall, and *F*-measure of the BN models were evaluated (Figure 16). The BN models obtained based on the K2 algorithm (Figure 17) were the highest for all parameters. Q_β was affected by kneading time (X_2) and had an effect on all granule properties. S_w was affected by water amount (X_1) and kneading time (X_2) and had an effect on all tablet properties. No links from the node of the amount of Mg-St (X_4) were observed.

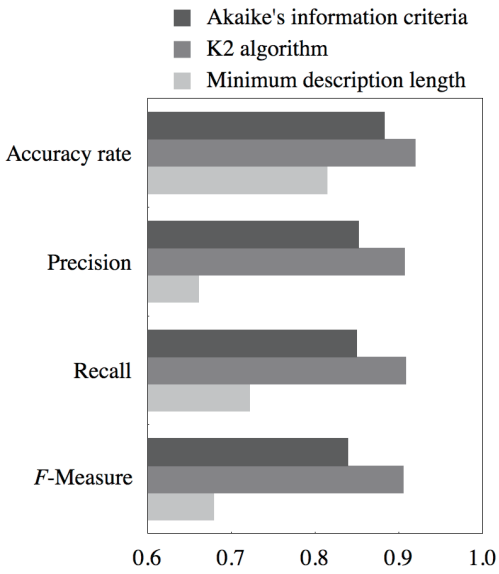

Fig. 16. Bayesian network model of the latent structure among process parameters, granule properties, and responses of tablets estimated using the K2 algorithm.

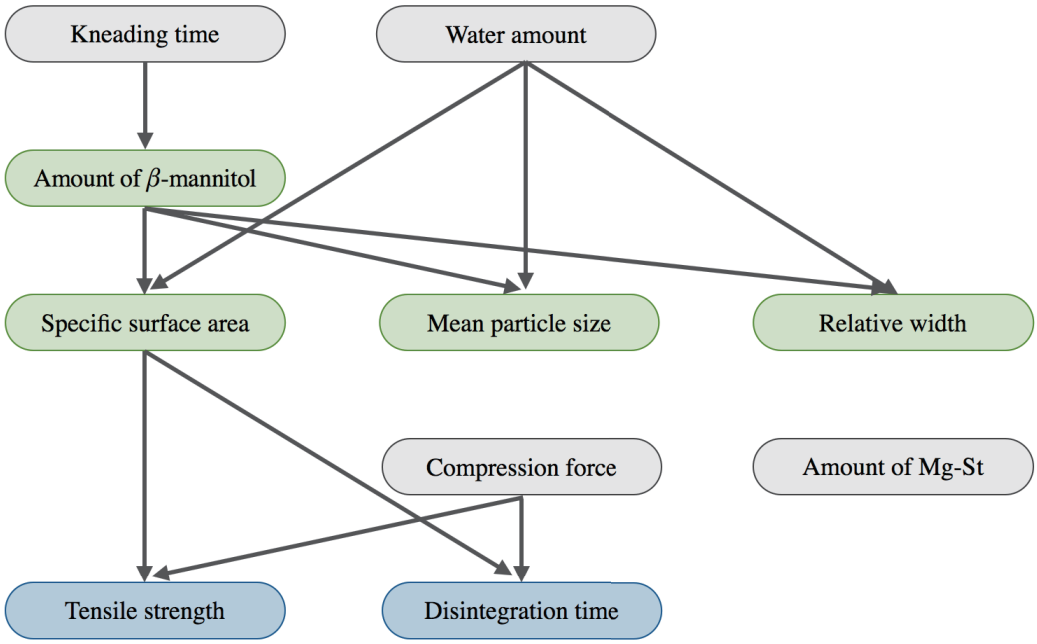

Fig. 17. Four standard measures of Bayesian network models based on each measurement criterion.

3.5. Evaluation of the causal relationships underlying the latent structure via probabilistic inference using a Bayesian network

Using BN modeling, the posterior probability of the causal factors was also predicted by conditional probability distributions (CPDs). To clarify the effects on Q_{β}, the posterior probabilities of the causal factors were predicted from Q_{β} and compression force (X_3). The BN model inferred factors with a short kneading time (X_2), low S_w, middle D_{50}, intermediate R_w, low TS, and short DT for tablets with an intermediate compression force (X_3) and a low Q_{β}. Conversely, the BN model inferred factors with an intermediate kneading time (X_2), high S_w, low D_{50}, high R_w, intermediate TS, and intermediate DT for tablets with an intermediate compression (X_3) force and a high Q_{β} (Figure 18).

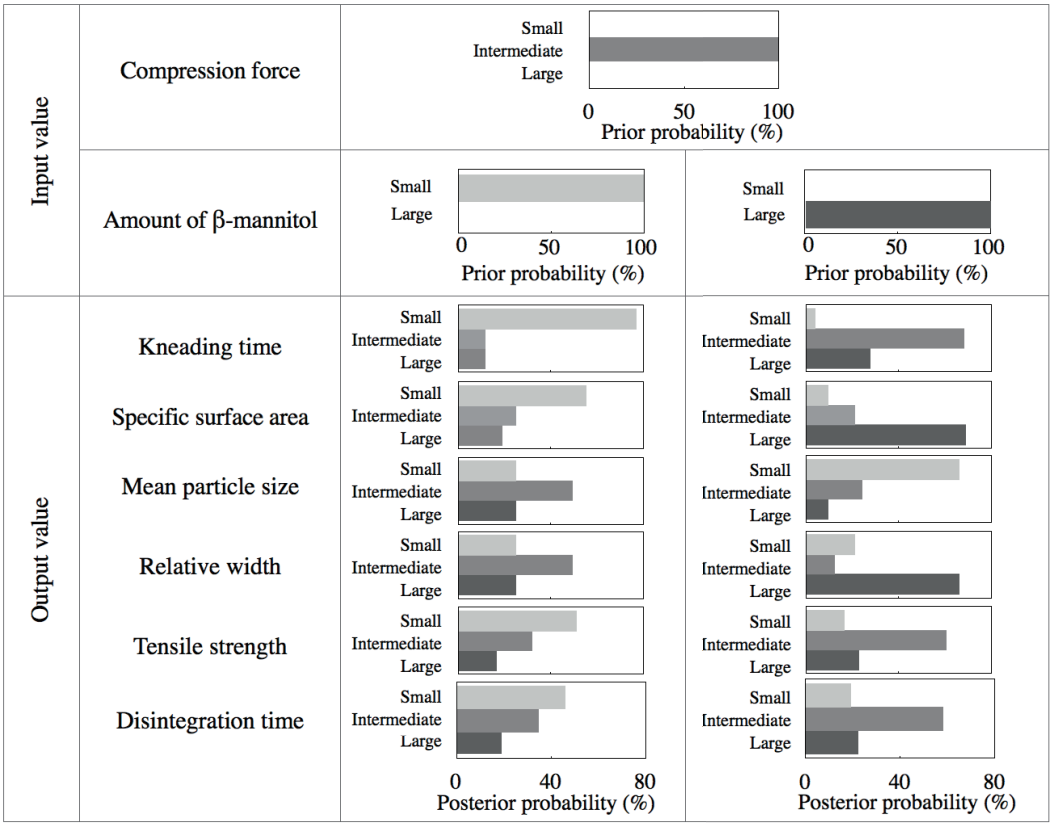

Fig. 18. Conditional probability distributions (CPDs) of causal factors inferred using a Bayesian network model. Compression pressure and amount of β-mannitol were set as prior probabilities. The CPDs of the causal factors were estimated for two cases: intermediate compression force and low amount of β-mannitol, and intermediate compression force and high amount of β-mannitol.

4. Discussion

In this study, tablets containing mainly mannitol, Cross-PVP, and MCC were prepared. Mannitol, Cross-PVP, and MCC were chosen as the filler, the disintegrating, and the binding agents, respectively.

Generally, ODTs are produced using a particular manufacturing method. Recently, it was reported that ODTs were also produced by a wet-granulation process using a polymorphic transition from the δ to the β form of mannitol.[52-53] In this study, we applied this technique to prepare ODTs.

We selected the amount of water (X_1) (as the granulation liquid), kneading time (X_2), compression force (X_3), and amount of Mg-St (X_4) as design variables. Water amount (X_1) and kneading time (X_2) may influence granule properties, such as Q_{β}, $S_{w,}$ d_{50}, and R_w, and have an indirect impact on tablet properties. Conversely, compression force (X_3) and amount of Mg-St (X_4) may also have a direct effect on tablet properties. When the water amount (X_1) reached ~45%, we could not prepare granules; therefore, the upper limit of the water amount (X_1) was set at 40%. A dissolution test revealed an absence of significant differences between Rp.13 and Rp.20. In contrast, Rp.13 and Rp.20 exhibited the lowest and longest disintegration times, respectively. This result suggests that all formulations tested have an excellent dissolution property. Therefore, we did not perform dissolution tests for the other formulations.

Response variables, such as Q_{β}, $S_{w,}$ d_{50}, R_w, TS, and DT, were predicted accurately using RSM-S, as shown clearly by the results of the LOOCV. Multiple regression analysis was also performed and the coefficient of determination, which was adjusted with degrees of freedom (R^{**2}) and is an indicator of the fit of each linear regression equation, was estimated. The R^{**2} values for Q_{β}, $S_{w,}$ d_{50}, R_w, TS, and DT were 0.712, 0.736, 0.747, 0.89, 0.861, and 0.699, respectively, resulting in poor estimations; a better result was observed using RSM-S.

The RSM is used widely to visualize the relationships between causal factors and responses. However, this method is limited to the three-dimensional (3D) space and includes basic information about the relationship between only two limited factors and one response. The Hyper-Dimensionally Embedded Cuboids (hyperDEC) technique has been developed as

a novel approach to visualize multivariable relationships. This method overcomes the limitation of the contour plots of 3D surface plots, which cannot display simultaneously the effects of more than two variables.[54] Using an approach similar to hyperDEC, we were able to viscerally and quantitatively understand the relationships between causal factors and responses (Figure 14). Both TS and DT increased with increasing water amount (X_1), kneading time (X_2), and compression force (X_3). TS surface was similar to DT, indicating that TS and DT were trade-off.

The relationship between two design variables and granule properties were clarified using RSM-S (Figure 15). Figure 15a suggests that a polymorphic transition from the δ to the β form of mannitol was induced by the wet-granulation process. A concomitant morphological change resulted in an agglomerate consisting of filament-like fine primary crystals (δ-granule). This phenomenon gave rise to an increase in S_w. Therefore, the Q_β surface was similar to the S_w, indicating that Q_β has a strong influence on S_w. Because S_w was affected not only by Q_β but also by water amount (X_1), kneading time (X_2), and d_{50}, the response surface for the S_w was barely different from Q_β.

BNs efficiently implement the probabilistic inference algorithm, which estimates the probability distribution of arbitrary random variables in a model.[55] To analyze the latent structure among causal factors, granule properties, and responses in ODTs, BN models were constructed using AIC, the K2 algorithm, and MDL as the judging criteria. The internal structures of BN models differed slightly depending on the judging criteria. Therefore, the optimal BN model was estimated using the indices accuracy rate, precision, recall, and *F*-measure (Figure 16). In general, there is a trade-off between precision and recall, as greater precision decreases recall and vice versa. The *F*-measure is the harmonic mean of precision and recall and considers both measures. All measures estimated using the model based on the K2 algorithm were more than 90% accurate, indicating that the prediction ability of the probabilistic model is sufficiently high. In contrast, all measures estimated using the model based on AIC and MDL were less than 90% accurate (Figure 16).

The distinctive probabilistic model was estimated by the edges, which represent conditional dependencies, and between the nodes, which represent the variables. The use of a BN model allowed the thorough understanding of the relationships among the variables of the manufacturing process and granule and tablet properties (Figure 17). As usual, TS and DT are strongly affected by the amount of Mg-St. However, no links between Mg-St (X_4) and TS or DT were observed, as shown in Figure 17. As shown in Figure 14, the effect of X_4 on TS and DT was rather weak compared with that of the other factors. This may be due to the limited amounts of Mg-St, which were ≤ 2.5%. Another explanation is that the powder sample used to prepare granules was small (200 g) in this study. It is well known that the lubricant effect of Mg-St is dependent on the scale of the samples.

Although S_w, d_{50}, and R_w were mutually dependent, in general, the BN model showed no significant effect of d_{50} and R_w on TS and DT. This result indicates that S_w is selected as a representative of granule parameters, such as d_{50} and R_w.

The CPDs of the factors of the ODTs were predicted using the BN model. The posterior probabilities of the factors for intermediate compression force and high and low Q_{β} were appropriately estimated (Figure 18). The BN model was able to estimate not only the effects of the causal factors on each response, but also the trends in the responses produced by the formulations as CPDs.

5. Conclusion

In this study, ODTs composed of IMC, mannitol, Cross-PVP, and MCC were prepared. The robustness of the response surfaces estimated via RSM-S was elucidated sufficiently, with high correlation coefficients observed in LOOCV. Optimal process variables were predicted quantitatively using RSM-S. Moreover, a latent structure analysis based on the variables of manufacturing process and granule and tablet properties was performed using BN. We visualized clearly the nonlinear relationships among the variables and identified several important correlations among them.

Chapter 4

Prediction of tablet characteristics from residual stress distribution estimated by the finite element method

1. Introduction

In previous chapters, I applied statistical techniques to pharmaceutical design. However, the mechanistic understanding of pharmaceutical unit operations is limited. In this chapter, I tried to apply numerical investigation to understand tableting process based on physical phenomenon.

Numerical investigation of the tableting process can assist in providing an understanding of the influence of tooling properties, lubrication and compaction kinematics (e.g., compaction speed and compaction sequences), and provide guidance for the optimization of tooling design and the improvement of powder formulation. One numerical analysis method is the finite element method (FEM), which is well established for the modeling of deformation of powders in various industries, such as compaction in ceramic industries, and analyzing pharmaceutical powder compaction.[56–57] In the FEM, powders are modeled as continuum media and the compaction behavior is analyzed by solving boundary value problems.

The Drucker–Prager Cap (DPC) model is one of the continuum mechanical models, in which the powder is considered a porous medium. The DPC model can represent the densification and hardening of the powder, as well as the interparticle friction.[58–59] The DPC model is therefore frequently used to analyze the strain, relative density changes and stress distribution of tablets during the tableting process.[60–62] The DPC model is characterized by parameters such as cohesion, internal friction angle, Young's modulus, Poisson ratio, parameters related to volume change and hardening mechanisms, and so on. In general, full calibration of the DPC model requires triaxial, hydrostatic compression and proportional loading tests. These tests are commonly used for metallurgical powders.[63–64] Because pharmaceutical powders are very soft and loosely packed, the application of triaxial cells in pharmaceutical materials is difficult. A shear cell test, which is based on the Mohr–Coulomb failure criterion, supplies data on the powder's cohesion and the friction angle at different pressures.[65–66] A direct shear test could also supply data on the cohesion and friction angle based on the Mohr–Coulomb failure criterion. In this study, volume change and hardening

law parameters were estimated using a response surface method that incorporated multivariate spline interpolation (RSM-S).

Several studies have reported that the residual stress distribution of tablets was estimated using the FEM, in which the powder is modeled using the DPC model. For instance, Han et al. have reported that density distributions of tablets were affected by punch geometry.[67] Tablet failure, in particular capping, is more likely to be associated with an intensive shear band formed during the decompression stage.[68–69] It has been shown that the density distribution patterns are comparable with the experimental results of others.[70–74]

The residual stress distribution of tablets might be affected by formulation and process variables. However, in the past, the influence of the residual stress distribution of tablets on characteristics of tensile strength (TS) and disintegration time (DT) has not been determined. The aim of this chapter was therefore to reveal differences in stress distribution between tablets composed of various formulations. Moreover, the predictive abilities of tablet characteristics of TS and DT on residual stress distribution were investigated.

Multiple linear regression analysis (MRA) and partial least squares (PLS) regressions were applied to determine the quantitative relationships between the stress distribution of tablets and the characteristics of TS and DT.

2. Materials and methods

2.1. Materials

Lactose (LAC; Tablettose 80, Meggle Japan Co. Ltd, Tokyo, Japan), cornstarch (CS; Graflow M, Nippon Starch Chemical Co. Ltd, Osaka, Japan) and microcrystalline cellulose (MCC; Ceolus PH-101, Asahi Kasei Chemicals Co. Ltd, Tokyo, Japan) were purchased. Magnesium stearate (Mg-St) was purchased from Wako Pure Chemical Industries Ltd (Osaka, Japan). LAC, CS, MCC and Mg-St were chosen as the filling, disintegrating, binding and lubricating agents, respectively.

2.2. Simulated conditions of the tableting process

Because the compaction of cylindrical tablets is an axisymmetric case, it can be analyzed using a two-dimensional FEM. Figure 19 shows the flow of the FEM; i.e., a FEM for modeling the compaction of flat-faced tablets, the model at the point of maximum compression and the model during decompression. The powder was exhibited as a DPC model. The die wall and upper punches were modeled as rigid bodies. The interaction between the powder, die wall and upper punch was modeled and the friction in the contacts was set to 0.195, in accordance with the reference.[19] The nodes on the symmetry axis were restricted to move only horizontally, and the nodes at the bottom boundaries were allowed to move only vertically. The upper punch could move vertically with compression.

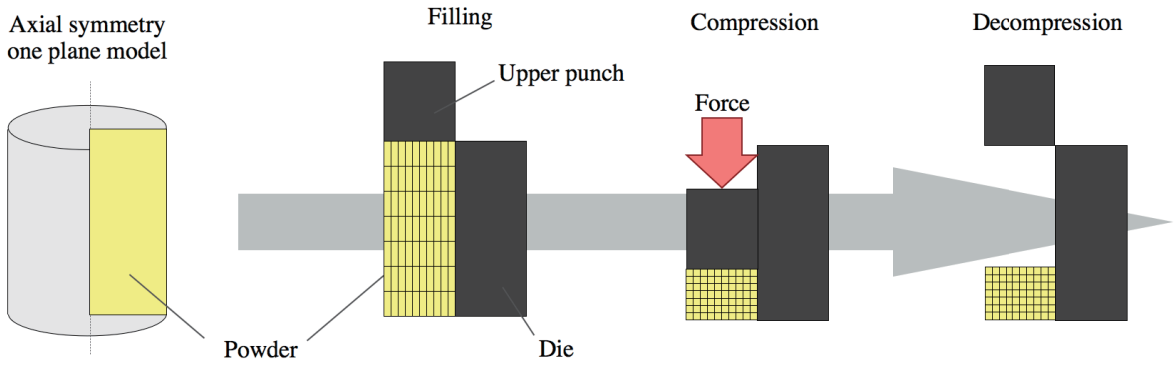

Fig. 19. Flow chart of the finite element analysis: a typical finite element model for modeling the compaction of flat-faced tablets, the model at the point of maximum compression and the model during decompression. The powder was modeled using the DPC model. An axisymmetric two-dimensional model (right half) was used.

2.3. DPC model

The DPC model was originally developed to predict the plastic deformation of soils under compression.[6–7] The model is formulated in terms of two invariants, l_1, the first invariant of the Cauchy stress, and J_2, the second invariant of the deviator stress. In terms of principal stresses, these invariants are given as:

$$l_1 = \sigma_1 + \sigma_2 + \sigma_3 \tag{12}$$

$$J_2 = \frac{1}{6}\{(\sigma_1 - \sigma_3)^2 + (\sigma_2 - \sigma_3)^2 + (\sigma_3 - \sigma_1)^2\} \tag{13}$$

where σ_1, σ_2 and σ_3 are the maximum, intermediate and minimum principal stresses, respectively, and compression is taken as negative.

Figure 20 shows the yield surface of the DPC model. It consists principally of three intersecting portions: a shear failure segment Y_s, a cap segment Y_c, and an expansion envelope portion Y_t, respectively. A typical geometrical shear envelope function is based on the exponential format given as:

$$Y_s(l_1, \sigma_0) = \sigma_0 - Ae^{(\beta^y l_1)} - \alpha^y l_1 \tag{14}$$

where σ_0 is the current cohesion related to a material constant. A, β^y and α^y are shear failure parameters. In this study, A and β^y were regarded as zero and the shear failure was represented as a simple linear model.

The cap segment that intersects the equivalent pressure stress axis is an elliptical curve with constant eccentricity in the I_1–J_2 plane, as given by:

$$Y_c(I_1, K_0, \sigma_1) = 1 - H(K_0 - I_1)\left\{\frac{I_1 - K_0}{R_c^y Y_s(K_0, \sigma_0)}\right\}^2 \quad (15)$$

where H is the Heaviside (or unit step) function. R_c^y is the ratio of elliptical x-axis to y-axis (I_1 to J_2). K_0 is the key flag, indicating the current transition point at which the compaction cap surface and shear portion intersect.

The expansion cap function Y_t is an elliptical function combined with the Heaviside function designed for the expansion cap, and is given by:

$$Y_t(I_1, \sigma_0) = 1 - H(I_1)\left\{\frac{I_1}{R_c^y Y_t(0, \sigma_0)}\right\}^2 \quad (16)$$

where R_c^y is the ratio of elliptical x-axis to y-axis (I_1 to J_2).

The cap hardening law is defined by describing the evolution of the parameter X_0, the intersection point of the compaction cap and the I_1 axis. The evolution of X_0 is related only to the plastic volume strain. The typical cap hardening law has the exponential form proposed by Fossum and Fredrich.[75]

$$\varepsilon_v^p = w_1^c\left[e^{\{D_1^c - D_2^c(X_0 - X_i)\}(X_0 - X_i)} - 1\right] \quad (17)$$

where X_i is the initial value of X_0 at which the cap takes effect in the plasticity model. W_1^c is the maximum possible plastic volumetric strain for geomaterials. Parameters D_1^c and D_2^c have units of 1/MPa and 1/MPa^2, respectively. In this study, D_2^c was regarded as zero and the hardening law was regarded as the simple model.

Moreover, the DPC model contains three parameters: Young's modules (E), the Poisson rate (υ) and the parameter related to the ratio of triaxial extension strength to compression strength (φ). When $\square = 0$, a yielding surface indicates the von Mises yield criterion.

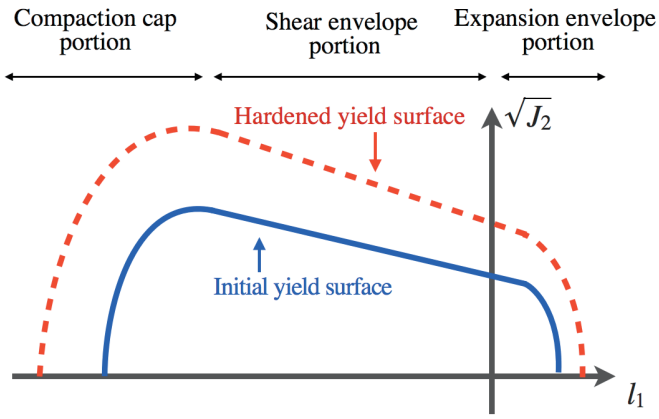

Fig. 20. A yield surface of the DPC model. The DPC model consists principally of three intersecting portions: an expansion envelope portion (Y_t), a shear failure segment (Y_s) and a cap segment (Y_c). In this study, a shear failure is regarded as a simple linear model.

2.4. Screening of DPC model parameters

A fractional factorial experimental design was used to evaluate the relative contributions of DPC model parameters. E, υ, R_c^y, R_t^y, X_i, σ_i, α^y, φ, W_1^c and D_1^c were selected as the causal factors affecting outputs such as volume change and maximum equivalent stress. One hundred twenty-eight kinds of DPC models were constructed. Levels in coded form and the exposition of each causal factor are summarized in Table 4. The constructed DPC model was fed into the analysis and the mechanical behavior of the powders during compaction was simulated using the FEM. To evaluate the significance of causal factors and their interactions, the data estimated using the FEM results were analyzed by analysis of variance (ANOVA).

Table 4. Level in coded form in ANOVA and exposition of each DPC model parameter

		Independent variables (DPC model parameters)	Level in coded form	
			1	2
E	:	Young's modules (GPa)	3	4
υ	:	Poisson rate	0.1	0.2
R_c^y	:	Ratio of l_1 to J_2 in compression	0.5	0.7
R_t^y	:	Ratio of l_1 to J_2 in tension	10	15
X_i	:	Initial value of cap intersection with l_1	$(-0.8e^{-3}) \times 3$	$(-1e^{-3}) \times 3$
σ_i	:	Parameter for initial cohesion value	$(8e^{-4})/\sqrt{3}$	$(1e^{-3})/\sqrt{3}$
α^y	:	Linear term for shear envelope	38	42
φ	:	Ratio of triaxial extension strength to compression strength	0.98	1
W_1^c	:	Max possible plastic volumetric strain	0.475	0.525
D_1^c	:	Cap hardening exponential term (units 1/MPa)	0.003	0.004

2.5. Preparation of model formulations

Model tablet formulations are shown in Fig. 21. Various amounts of LAC, CS, and MCC were selected as the formulation factors. Based on preliminary experiments, the lower and upper limits of the levels of each factor were set.

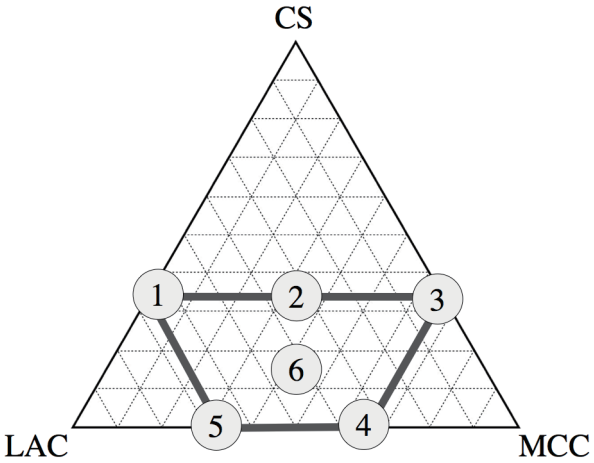

Fig. 21. Six model formulations composed of LAC, CS and MCC. LAC, CS and MCC were chosen as the filler, the disintegrating and the binding agents, respectively. Each number indicates formulation numbers, respectively.

2.6. Measurement of a failure envelope using the direct shear test

A direct shear tester (NS-V100, Nanoseeds Corporation, Gifu, Japan) was used to measure the failure envelope and estimate the two DPC model parameters of α^y and σ_i. Before measurement, all ingredients were dried at 75°C for 12 h. Powder (20 g) was added into the shear cell. Precompression was performed consecutively at 50 and 45 N. Shear stresses were then measured when the powder bed was compressed at 20, 30 and 40 N, respectively. Data observed were plotted in the axial shear (σ)-stress (τ) plane. The linear approximation method was applied to estimate a failure envelope. The failure envelope was measured for six powders of each formulation.

To obtain the internal friction angle (α^y) and cohesion (σ_i) in the equivalent stress (p)–hydrostatic stress (q) plane, a Mohr's circle that touched the failure envelope in the σ–τ plane was estimated (Fig. 22). Two intersections between the Mohr's circle and the x-axis were then calculated. These values indicate the maximum and minimum principal stress (σ_1 and σ_3) in triaxial compression status, respectively:

$$\sigma_a = \frac{\sigma_1+\sigma_3}{2} - \frac{\sigma_1-\sigma_3}{2}\sin\theta \tag{18}$$

$$\tau_a = \frac{\sigma_1-\sigma_3}{2}\cos\theta \tag{19}$$

where σ_a and τ_a are the points on the failure envelope, and θ is the internal friction angle in the σ–τ plane.

For this study of the direct shear test, using uniaxial compaction in a cylindrical die in the z-direction, the following assumptions can be made:

$$\sigma_1 = \sigma_z \tag{20}$$

$$\sigma_2 = \sigma_3 = \sigma_\tau \tag{21}$$

We therefore have:

$$p = \frac{(\sigma_z-2\sigma_\tau)}{3} \tag{22}$$

$$q = \frac{|\sigma_z-\sigma_\tau|}{\sqrt{2}} \tag{23}$$

Data observed were plotted in the p–q plane and a linear approximation method was applied to estimate the failure envelope. The gradient and y–intercept of the failure envelope

indicated the internal friction angle β_i and cohesion d_i in the p–q plane, respectively. α^y and σ_i are defined as:

$$\alpha^y = \frac{\sqrt{3}\tan\beta_i}{3} \tag{24}$$

$$\sigma_i = \frac{d_i e^{-3}}{\sqrt{3}} \tag{25}$$

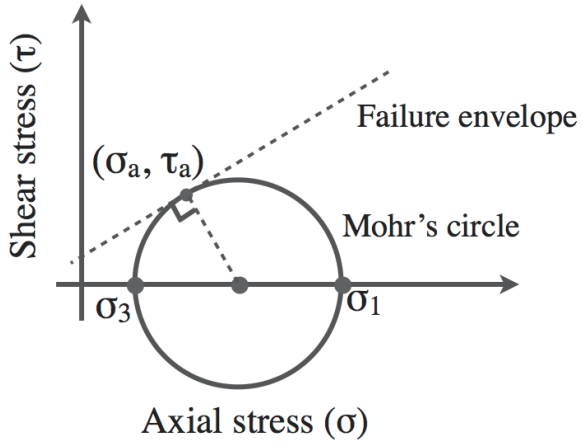

Fig. 22. Mohr's circle contacted failure envelope in the axial–shear stress plane. The maximum and minimum principal stresses were estimated from two intersections between the Mohr's circle and the x-axis.

2.7. Preparation of tablets

All ingredients were dried at 75°C for 12 h. The ingredients were weighed accurately according to the experimental formulations, and all ingredients were blended in a polyethylene bag for 2 min. The final blend was compressed directly into flat-faced tablets (200 mg, 8 mm diameter) using a tableting machine (AUTOTAB-500; Ichihashi-Seiki Company Ltd, Kyoto, Japan). All formulations comprised 198 mg of a mixture of LAC, CS, and MCC, and 2 mg of Mg-St.

2.8. Estimation of DPC model parameters using volume change as output

A statistical method was applied to estimating the two DPC model parameters (W_1^c and D_1^c) using volume change as an indicator. Tablets compressed at 4, 5, 6, 7, 8, 9 and 10 kN were prepared and the thickness of tablets was measured. The W_1^c and D_1^c were assigned to 3^2 full factorial designs, and nine kinds of DPC models were constructed for each formulation.

The range of these parameters was determined by a preliminary test. Values of α^{y} and σ_i were obtained from the direct shear test measurements. E, υ and R_c^{y} were determined based on references [19]; i.e., E = 3.57 GPa, υ = 0.12 and R_c^{y} = 0.6. R_t^{y} = 10, X_i = 0.1 and φ = 1 were set as arbitrary values, which do not cause divergence problems in FEM analysis. The tableting process was simulated using the FEM and measured the thickness of tablets after decompression at each compression force. Data observed were modeled by RSM-S, and DPC model parameters correlated with the experiment were estimated.

2.9. Measurement of hardness and DT

The hardness of the tablets was determined using a tablet hardness tester (Ogawa Seiki Co., Tokyo, Japan). TS was calculated using Eq. (1). TS values for six tablets of each formulation were measured.

The disintegration test was performed according to the JP16 disintegration test for tablets using a disintegration tester (NT-20H; Toyama Sangyo Co. Ltd, Osaka, Japan) and water (as a test medium) at 37°C. The DT was defined as the interval required for the complete disappearance of a tablet or its particles from the tester net. The DT was measured for six tablets of each formulation.

2.10. Modeling of causal relationships between residual stress distribution and tablet characteristics

MRA was performed to clarify causal relationships between the residual stress distribution of tablets and responses of the tablet. Nine typical points of the stress distribution of tablets were selected as explaining variables. The TS and DT were selected as responses of tablets. A forward selection method based on stepwise selection was applied to the selection of causal factors and factors showing p values larger than 0.25 were successively excluded from analysis.

A PLS regression was used to examine the relationships in more detail. PLS calibration models were evaluated using the leave-one-out cross-validation (LOOCV) method. Data

composed of *x*-axial, *y*-axial or shear stress distributions were selected as explaining variables. Each stress distribution contained 1532 data points. The TS and DT of tablets compressed at 5, 7 or 9 kN were selected as output variables. Thirty-six samples in total were used for PLS regression analysis in each model. The optimum number of factors was taken to be that leading to a minimum value in the predicted residual error sum of squares (*PRESS*) versus a PLS component graph, the former being defined as:

$$PRESS = \sum_{i=1}^{n} (\hat{y}_i - y_i)^2 \quad (24)$$

where $\hat{y}_i$ and y_i correspond to the TS or DT values of each sample predicted by the residual stress distribution and experiment, respectively.

The goodness of calibration and prediction was assessed in terms of the root mean square error (RMSE), which was termed RMSEC for calibration and RMSEP for prediction:

$$\mathrm{RMSE} = \sqrt{\frac{\sum_{i=1}^{n} (\hat{y}_i - y_i)^2}{n}}. \quad (25)$$

2.11. Computer programs

The FEM analysis of the tableting process was performed using ANSYS® 13.0 (ANSYS Inc., Canonsburg, PA, USA). The RSM-S was performed using dataNESIA® version 3.2 (Azbil Corporation, Fujisawa, Japan). The ANOVA and MRA were performed using JMP version 8 (SAS Institute Inc., Cary, NC, USA). The chemometric analysis was performed using the PLS regression program associated with the Unscrambler 9.0 software (CAMO Technologies, Inc., Woodbridge, NJ, USA).

3. Results and discussion

3.1. Screening of DPC model parameters

The ANOVA was performed to investigate the influence of DPC model parameters on the volume change and stress distribution of tablets. As shown in Table 4, the ranges of each of the DPC model parameters were decided based on the previous literature.[19] Values of parameters were set with a relatively small range because values that are too high or too low may cause divergence of iterative calculations. Results of the ANOVA revealed that 15 and 14 factors significantly affect the volume change (tablet thickness) and the residual stress of the tablets, respectively. These results are shown in Tables 5 and 6. The volume change and hardening law were significantly affected by W_1^c and D_1^c, and the residual stress of tablets was significantly affected by the internal friction angle (α^y) and Young's modules (E). The hardening law in the DPC model generally refers to the evolution of the cap surface with the volumetric plastic strain defined. The W_1^c and D_1^c are parameters related to the volumetric plastic strain. The E and α^y parameters are related to elastic deformation and internal friction of powder, respectively.

Table 5. ANOVA results for tablet thickness

Factor/Interaction	*F* value	*p* value
W_1^c	213507	< 0.0001*
D_1^c	119816	< 0.0001*
E	30866	< 0.0001*
α^y	10885	< 0.0001*
φ	707	< 0.0001*
$E \times \alpha^y$	629	< 0.0001*
R_c^y	605	< 0.0001*
$\alpha^y \times W_1^c$	69	< 0.0001*
$E \times D_1^c$	67	< 0.0001*
$E \times W_1^c$	61	< 0.0001*
$W^c{}_1 \times D_1^c$	44	< 0.0001*
$E \times R_c^y$	42	< 0.0001*
$R_c^y \times \alpha^y$	37	< 0.0001*
$R_c^y \times D_1^c$	18	< 0.0001*
$E \times \varphi$	10	0.0021*

Table 6. ANOVA results for equivalent stress

Factor/Interaction	*F* value	*p* value
α^y	2285	< 0.0001*
E	2239	< 0.0001*
$E \times \alpha^y$	672	< 0.0001*
W_1^c	220	< 0.0001*
R_c^y	141	< 0.0001*
φ	138	< 0.0001*
$\alpha^y \times \varphi$	32	< 0.0001*
$\alpha^y \times D_1^c$	27	< 0.0001*
$E \times R_c^y$	19	< 0.0001*
$E \times D_1^c$	16	0.0002*
$E \times W_1^c$	11	0.0012*
$W_1^c \times D_1^c$	6	0.0154*
D_1^c	6	0.0211*
$R_c^y \times W_1^c$	5	0.0225*

3.2. Measurement of the internal friction angle and cohesion

Figure 23 shows the results of the internal friction angle and cohesion in the σ–τ plane. The α^y and σ_i values were found to vary from 4° to 47° and 0.78 kPa to 11.5 kPa, respectively. The internal friction angle increased as the amount of MCC increased. The tablet with the largest amount of MCC (Rp. 3, 4 and 5) showed the highest internal friction angle value. In contrast, the powder composed of only CS and LAC (Rp. 1) had the lowest internal friction angle value. The tablet with the largest amount of MCC (Rp. 4) showed the highest value of cohesion. On the other hand, the tablet composed of only CS and MCC (Rp. 3) showed the lowest value of cohesion. The values of α^y and σ_i were similar to those of the failure envelope in the σ–τ plane.

The effect of the E value on the residual stress distribution was comparable to α^y, as shown in Table 6. Parameter values in the ANOVA were set with a relatively small range because values that are too high or too low may cause divergence of iterative calculations. The α^y, in particular, causes divergence of iterative calculations. However, although the α^y value was set from 38° to 42° in the ANOVA, the α^y was found to vary from 4° to 47° by direct shear test. On the other hand, it is likely that the E value varied from 1 to 6, at most. For example, the E value of lactose compressed at 200 and 250 MPa showed 3.5 and 4.6 GPa, respectively.[59, 65] The E value of the mixture composed of lactose, cornstarch and MCC at 100 MPa varied from approximately 0.1 to 1.5 GPa.[76] The results of the direct shear test and the range of parameters suggested that the residual stress might be strongly affected by α^y, so E was set as a constant.

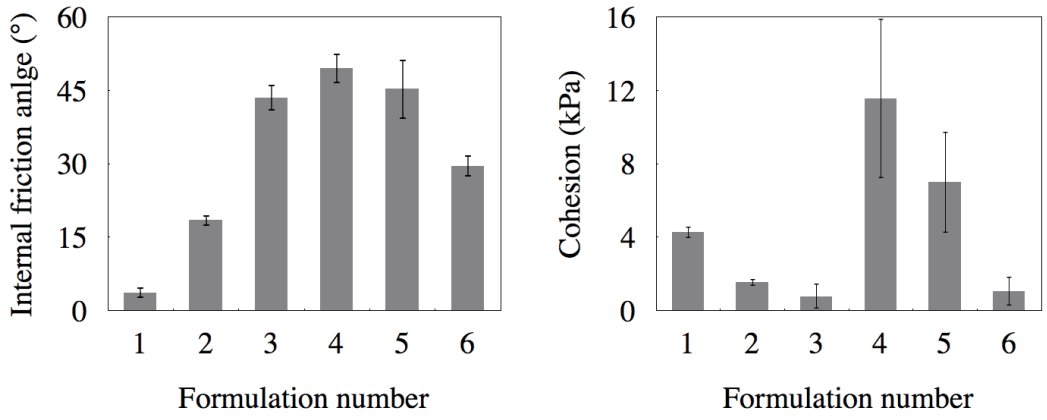

Fig. 23. Results of a direct shear test: (a) the internal friction angle and (b) the cohesion of each model formulation.

3.3. Estimation of the hardening law parameters using volume change

The combined technique of a factorial experimental design and RSM-S was applied to determine the volume change and hardening law parameters (W_1^c and D_1^c). The volume of each formulation weighing 200 mg is shown in Table 7. The powder composed of only the CS and MCC (Rp. 3) showed the highest bulk density. In contrast, the powder composed of only the CS and LAC (Rp. 1) had the lowest bulk density.

The thickness of tablets varied from 3.41 mm to 3.84 mm, and from 3.25 mm to 2.96 mm when tablets were compressed at 4 kN and 10 kN, respectively. When the compression force was 4 kN, the thickness was in the order of Rp. 3 > Rp. 2 > Rp. 6 > Rp. 4 > Rp. 5 > Rp. 1. In contrast, the thickness at 10 kN was in the order of Rp. 3 > Rp. 2 > Rp. 1 > Rp. 6 > Rp. 4 > Rp. 5.

Tablet thickness was accurately predicted by the DPC model parameters (W_1^c and D_1^c) using RSM-S, further suggesting that tablet thickness decreased with increasing W_1^c and D_1^c. The optimum DPC model parameters are summarized in Table 7. To validate the optimum DPC model parameters, the tableting process was simulated using the FEM. The tablet thickness simulated by the FEM was compared with experimental values, indicating a good linear relation with sufficiently high correlation coefficients from .94 to .98. Moreover, the

RMSE values ranged from .01 to .03, indicating sufficiently low prediction error. This result suggests that W_1^c and D_1^c correlated well with tablet thickness.

Table 7. DPC model parameters determined by experiments

Rp.	Thickness of powder bed (mm)	α^y	σ_i	W_1^c	D_1^C
1	6.560	4.352	4.283	0.699	0.010
2	8.636	22.187	1.545	0.967	0.011
3	9.626	44.621	0.782	1.083	0.012
4	9.458	47.807	11.573	1.129	0.015
5	8.090	45.408	6.995	0.990	0.012
6	8.301	33.956	1.070	0.997	0.011

3.4. Simulation of the tableting process and estimation of the residual stress distribution of tablets

The material properties calibrated from experiments were fed into the ANSYS software in which the DPC model was implemented. The DPC model parameters are shown in Table 4. In this study, appropriate values of the parameters E, v, R_c^y, R_t^y, X_i and φ were sought in an arbitrary manner when they could not be measured by the data.

Although the residual stress distribution was accurately estimated using the DPC-based FEM 2D model, there are limitations of applying a two-dimensional FEM to an asymmetrical model, such as a caplet or stamped tablet.

Figure 24 shows a typical residual stress distribution of tablets. In x axial stress (σ_x), the top corner had the highest value while the bottom had the lowest. It is clear that the absolute value of y axial stress (σ_y) at the top was generally lower than that at the bottom. Moreover, the σ_y value at the top had the stress extending upward while the bottom had the stress extending downward. When the applied force from the upper punch was removed, a large σ_y value at the top central region was brought about by radial elastic recovery, while most of the other regions were still constrained by die walls. At the same time, the σ_x value became

enlarged at the top central and bottom peripheral regions. Results of the shear stress (τ) revealed that an intensive shear region was recognized from the top edge to the mid-center. In this shear region, the shear stress changed from positive to negative, indicating a change in the direction of the shear stress. For instance, when the applied force from the upper punch was removed, the radial elastic recovery of the material at the top central region caused large shear stresses because most of the other regions were still constrained by die walls, and therefore the axial and shear stresses at the top corner of the tablets were larger than those in peripheral regions. This result is consistent with previous findings.[77]

Although the residual stress distribution is similar among model formulations, the ranges of stress values were significantly different. For instance, σ_x, σ_y and τ values of the Rp. 2 were higher than those of the other formulation. The large τ values were located near the die edge in Rp. 2, although the value was rather uniform in the other formulations. In general, shear deformation in granules is induced by the dilation of materials. Eccentrically located stress in the tablet may cause edge chipping, capping and lamination failure. These have been demonstrated experimentally as typical failure patterns in the tableting process.[20] It is likely that the tablet made by Rp. 2 had such tableting problems.

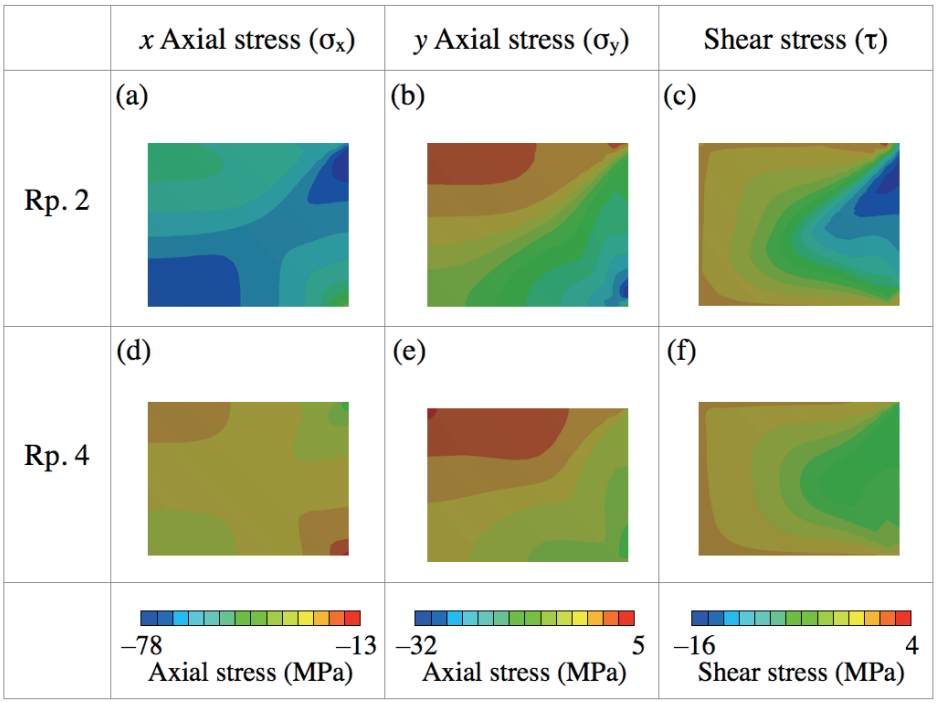

Fig. 24. Two-dimensional maps for the residual stress distribution of tablets estimated using the FEM: (a) x axial stress (σ_x), (b) y axial stress (σ_y) and (c) shear stress (τ) of Rp. 2. (d) x axial stress (σ_x), (e) y axial stress (σ_y) and (f) shear stress (τ) of Rp. 4.

3.5. TS and DT results

TS and DT were displayed using response surfaces, which were estimated by RSM-S. The accuracy of each response surface was evaluated by LOOCV, and correlation coefficients for prediction were sufficiently high (.90 to .97). Response surfaces of the TS and DT of tablets compressed at 9 kN are shown in Fig. 25. The TS increased as the amount of CS decreased (Fig. 25a). A much higher TS value was observed for tablets containing low and high amounts of CS and MCC. The tablets with the largest amount of MCC, and with no MCC, exhibited high value of DT, while other tablets showed low value of DT (Fig. 25b).

DT increased with increasing TS. However, the tablet composed of only CS and LAC resulted in exceptionally high DT but low TS, indicating that MCC acts not only as a binder, but also as a disintegration agent.

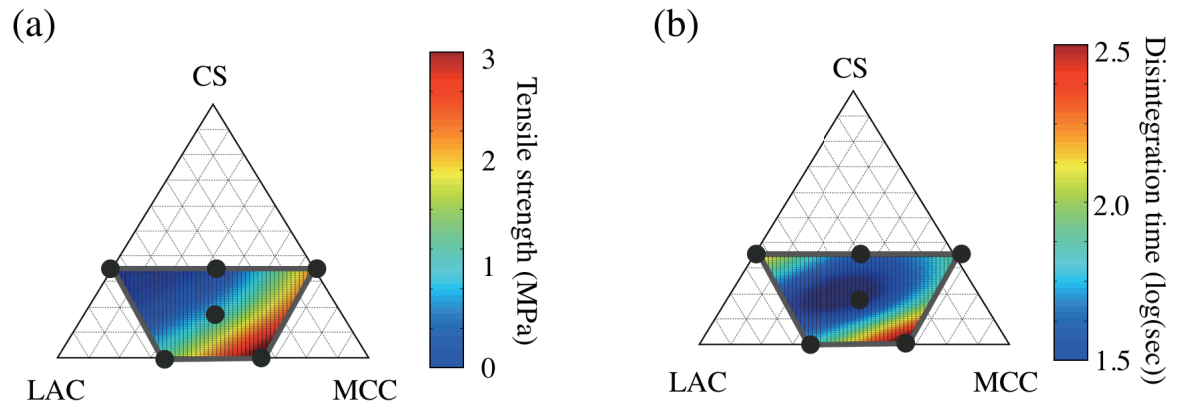

Fig. 25. Response surfaces estimated by RSM-S for (a) TS and (b) DT of tablets compressed at 9 kN.

3.6. Prediction of tablet characteristics based on the residual stress distribution of tablets

MRA was used to clarify the relationship between the residual stress distribution and tablet characteristics. The forward selection method, based on a stepwise selection, revealed that TS and DT were affected significantly by 16 and 15 factors, respectively. A coefficient of determination, which was adjusted with degrees of freedom (R^{**2}), an indicator of the fit of each linear regression equation, was estimated. The R^{**2} of the TS and DT showed .992 and .942, respectively, and the RMSE of the TS and DT showed .080 and .082, respectively. This result suggests that the residual stress distribution of tablets is a good estimator for TS and DT.

Figure 26 shows the intensity of the residual stress distribution of tablets, which gives high TS and DT. Horizontal and vertical arrows show the intensity of x and y axial stresses. Circles indicate shear stresses. Blue arrows and circles indicate that the TS or DT was small when the stress was close to zero. In contrast, red arrows and circles indicate that the TS or DT became large when the stress deviated from zero. The MRA revealed that TS was strongly affected by σ_y values at mid-center and τ values at top-center. On the other hand, DT was affected significantly by σ_x values at the top-center and bottom-corner, and τ values at top-center. In terms of the rule of common sense, it is recognized that a homogeneous distribution of residual stress is important to enhance TS. However, MRA results revealed that in some cases, heterogeneous distribution of residual stress might enhance TS.

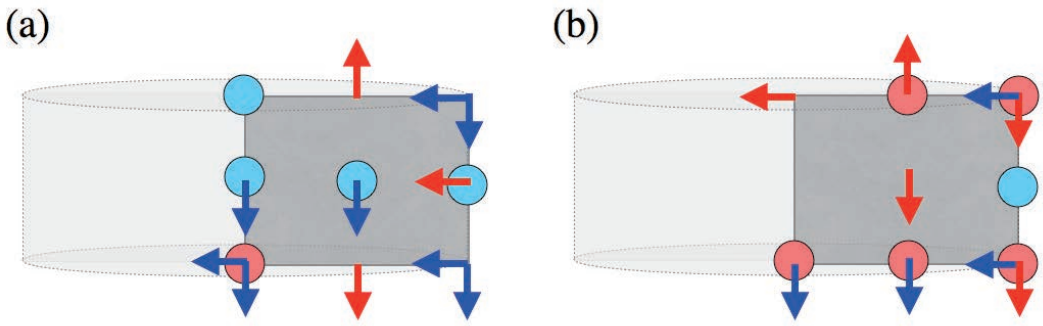

Fig. 26. Two-dimensional maps for the residual stress distribution of tablets resulting in high (a) TS and (b) DT. Horizontal and vertical arrows indicate x and y axial stress (σ_x and σ_y), respectively. Circle indicates shear stress (τ). Blue arrows indicate that TS or DT values become small when this stress is close to zero. Red arrows indicate that TS and DT values become large when the stress deviates from zero.

PLS regression was performed to understand further details of the influence of formulation factors on residual stress distribution. Calibration models for the TS and DT of tablets compressed at 5 kN were estimated using PLS. Statistical indices such as R^2 (a determination coefficient), *RMSEC* and *RMSEP* of the calibration model for the TS were .95, .081 and .095, respectively, and those of the DT were .903, .085 and .100, respectively. Therefore, both TS and DT were predicted well with high accuracy from σ_x, σ_y and τ values in tablets, suggesting that residual stress distribution can be used as CQAs in pharmaceutical development. To reveal the degree of incidence, two-dimensional maps of regression coefficients are shown in Fig. 27. The results revealed σ_x at the top corner, σ_y at the mid-center and τ at the bottom corner were very sensitive to the TS, and σ_x at the top-middle, σ_y at the bottom-corner and τ at the bottom-corner had a significant influence on DT. This study clearly revealed that the residual stress distribution in the tablet became a significant contributor to the characteristics of TS and DT, although further investigation is needed to understand the detailed mechanism of these stress parameters.

To control the residual stress distribution using the FEM, we could design an optimum tablet formulation with excellent pharmaceutical responses, such as high tensile strength and short disintegration time. Controlling the residual stress distribution leads not only to the

design of the optimum formulation and process variables, but also allows the mechanisms of the pharmaceutical responses of the tablet to be understood.

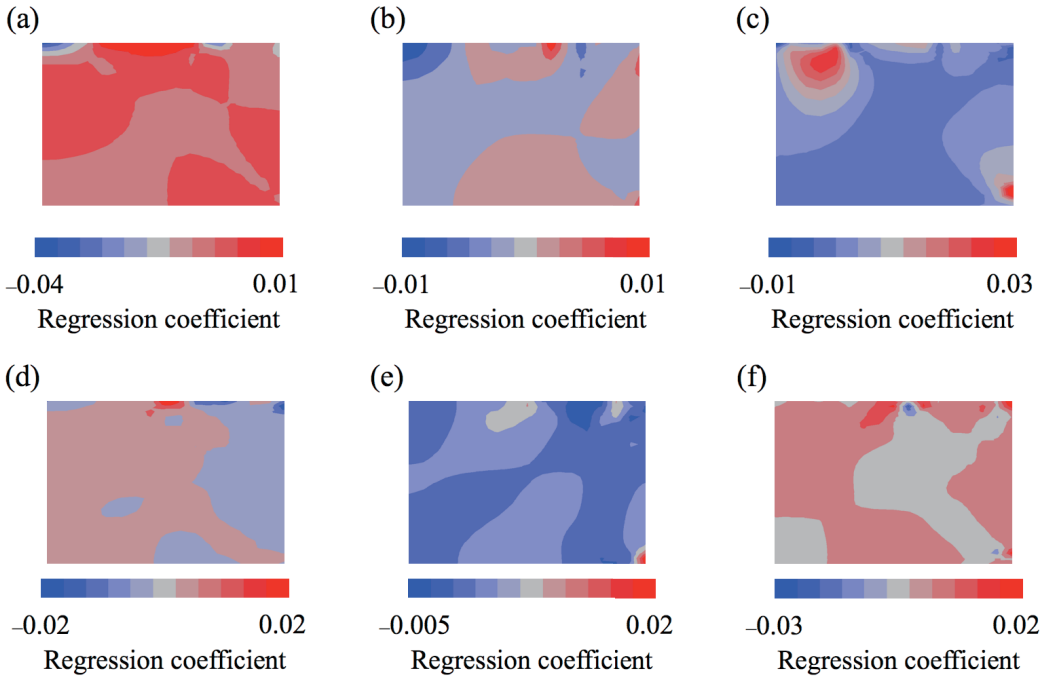

Fig. 27. Two-dimensional maps for regression coefficients in PLS analysis for TS and DT using LOOCV. A series of residual stress distribution data was employed as explaining variables in PLS. (a) x axial stress (σ_x), (b) y axial stress (σ_y) and (c) shear stress (τ) in PLS analysis of TS. (d) x axial stress (σ_x), (e) y axial stress (σ_y) and (f) shear stress (τ) in PLS analysis of DT.

4. Conclusion

A direct shear test and RSM-S were applied to model the mechanical behavior of pharmaceutical powders composed of LAC, CS and MCC, based on the DPC model. The FEM was used to simulate compaction behavior of the powders. The numerical results revealed that the residual stress distribution of tablets was affected by formulation and compression force. In particular, the residual stress distribution of tablets composed of equal amounts of LAC, CS and MCC was more uniform than the tablets composed of 67% MCC and 33% LAC, with no CS. Results of the MRA and PLS regression demonstrated that the residual stress distribution of tablets was closely related to the characteristics of TS and DT. In conclusion, the residual stress distribution of tablets simulated by the DPC model using the FEM might be useful as novel CQAs in pharmaceutical development.

Summary

When designing pharmaceutical products, the relationships between causal factors and pharmaceutical responses are intricate. Therefore, the formulators' expertise and experience are essential in designing an acceptable product formulation. The empirical approach requires a prolonged development time and significant resources. In recent years, regulatory authorities such as the US Food and Drug Administration and the International Conference on Harmonisation (ICH) have promoted and requested the application of quality-by-design (QbD) principles to facilitate the exchange of complex information about chromatographic selectivity and critical resolution values to support better method control, including method transfer. In particular, according to the ICH Q8 guidelines, a scientific understanding of the formulation and manufacturing method is required.

In recent years, statistical approaches have been used for seeking acceptable formulations of pharmaceuticals. Response surface method (RSM) includes statistical factorial experimental design, modeling between causal factors and response variables, and multi-objective optimization for selecting the best formulation under a set of experimental restrictions. Predictions based on traditional linear regression models are often limited and the results obtained occasionally exhibit poor estimation. On the other hand, there are advantages in the precise prediction of the optimal solution using the non-linear techniques, RSM-S. However, several difficulties are yet to be overcome regarding a non-linear technique such as RSM-S. For instance, no proper method of analyzing the relationships of the latent structure among the design variables and response variables, and evaluating the reliability of border of design space (DS) estimated by RSM-S. Moreover, the mechanistic understanding of pharmaceutical unit operations is limited. The purpose of this study was to overcome these problems and establish a valuable method.

In Chapter 1, a Bayesian network (BN) was used to clarify the latent structure underlying the causal factors and pharmaceutical responses of a tablet containing solid dispersion (SD) of indomethacin (IMC). BN is a directed acyclic graphical approach that expresses the

probabilistic causal relationships among attributes, in which probabilistic relationships are expressed by nodes and the links connecting the nodes. In this chapter, I successfully determined the complex relationships between causal factors and pharmaceutical responses using BN modeling. Moreover, both the causal factors and responses were predicted by the BN model using conditional probability distributions (CPDs).

Using RSM-S, we can understand nonlinear relationships between causal factors and response variables, and can estimate the high-integrity design space. However, the reliability of the nonlinear response surface estimated by RSM-S cannot be evaluated directly using conventional statistical quantities. In Chapter 2, a resampling method with replacement was applied to evaluate the reliability of border on the design space estimated by RSM-S and nonlinear design space considered reliability of border was set upped. The resampling method with replacement for statistical inference is a nonparametric approach to compute estimated standard errors, confidence intervals and hypothesis testing. I revealed RSM-S and this resampling method might be useful for estimating the reliability of nonlinear design space.

A key goal of QbD is to identify the most important critical quality attributes (CQAs) and to understand their relationships with the product performance. It is needed to clarify the relationships among the variables, intermediates in-process materials, and pharmaceutical characteristics because the intermediates in process could be CQAs. In Chapter 3, a multivariate statistical technique was applied to the design of an orally disintegrating tablet and to clarify the causal correlation among variables of the manufacturing process and pharmaceutical responses. Orally disintegrating tablets (ODTs) composed mainly of mannitol were prepared *via* the wet-granulation method using crystal transition from the δ to the β form of mannitol. A latent structure analysis of the pharmaceutical formulations of the tablet performed using a Bayesian network led to the clear visualization of a causal connection among variables of the manufacturing process and tablet characteristics. This technique provides a better understanding of the complicated latent structure among variables of the manufacturing process and tablet characteristics.

In previous chapters, statistical techniques were applied to pharmaceutical design. However, the mechanistic understanding of pharmaceutical unit operations is limited. In Chapter 4, numerical investigation was used to pharmaceutical design. Tablet characteristics of tensile strength and disintegration time were predicted using residual stress distribution, simulated by the finite element method (FEM). The Drucker–Prager Cap (DPC) model was calibrated using a direct shear test and analysis of the hardening law of the powder. The constructed DPC model was fed into the analysis using the FEM, and the mechanical behavior of pharmaceutical powders during compaction was analyzed using the FEM. The tensile strength and disintegration time were predicted accurately from the residual stress distribution of tablets using multiple linear regression analysis and partial least squares regression analysis. This suggests that the residual stress distribution of tablets is related closely to the tensile strength and disintegration time.

In conclusions, these findings suggest that proposed novel multivariate statistical approaches and numerical analysis method are useful tools for the pharmaceutical design under the QbD concept.

Acknowledgements

First of all, I would like to express my gratitude and deepest appreciation to Professor Kozo Takayama for his guidance and advice in my research work and preparing this dissertation.

Secondly, I would like to also express my great appreciation to Dr. Yasuko Obata and Dr. Yoshinori Onuki for their helpful guidance and assistance in my research work.

Also, I wish to thank Dr. Shingo Kikuchi, Mr. Akihito Yasuda, Mr. Keisuke Takagaki, Dr. Masato Nishikawa, Dr. Hiroshi Watanabe (Department of Pharmaceutics, Hoshi University), Takahiro Miura (Cybernet Systems Co., Ltd.,), Dr. Hiroaki Arai, Dr. Jin Maeda (Daiichi Sankyo Co., Ltd.), Dr. Tadashi Norioka (Astellas Pharma Inc.) and Dr. Yasuhiro Shimada (Nano Seeds Corporation) for their valuable suggestions and fruitful discussions.

In addition, I am grateful to Mr. Shota Kawai, Mr. Hiroshi Mochida, Ms. Etsuko Oshima, Ms. Maho Taniguchi, Ms. Saori Otoguro, Mr. Naoto Uehara, Mr. Tatsuya Nakamura, Mr. Shozo Iwasaki, Ms. Kaori Chou, and all my colleagues of the Department of Pharmaceutics of Hoshi University for their kindness and assistance.

Moreover, I would like to also express my great appreciation to Professor Makoto Otsuka (Faculty of Pharmacy, Research Institute of Pharmaceutical Science, Musashino University), Yoshihiro Tokudome (Faculty of Pharmaceutical Sciences, Josai University), Hiroshi Uchida (Kyorin Pharmaceutical Co., Ltd.) and Takaya Sato (CAMO Software Japan Co., Ltd.) for their a lot of kindly assistance and encouragement.

Finally, I wish to express my sincere gratitude to my wife, parents, brother and sister. This thesis would not have been fulfilled without their encouragement and support of my study and life.

References

1. Jivraj, M., Martini, L. G., Thomson, C. M., An overview of the different excipients useful for the direct compression of tablets, *Pharm. Sci. Technolo. Today*, **3**, 58–63 (2000)
2. Onuki, Y., Kawai, S., Arai, H., Maeda, J., Takagaki, K., Takayama, K. Contribution of the physicochemical properties of active pharmaceutical ingredients to tablet properties identified by ensemble artificial neural networks and Kohonen's self-organizing maps, *J. Pharm. Sci.*, **101**, 2372–2381 (2012)
3. International Conference on Harmonization of Technical Requirements for Registration of Pharmaceuticals for Human Use (August 2009). Pharmaceutical Development - Q8 (R2). http://www.ich.org/products/guidelines/quality/article/ quality-guidelines.html
4. International Conference on Harmonization of Technical Requirements for Registration of Pharmaceuticals for Human Use (November 2005). Quality Risk Management - Q9. http://www.ich.org/products/guidelines/quality/article/ quality-guidelines.html
5. International Conference on Harmonization of Technical Requirements for Registration of Pharmaceuticals for Human Use (June 2008). Pharmaceutical Quality System - Q10. http://www.ich.org/products/guidelines/quality/article/ quality-guidelines.html
6. Khuri, A. I., Cornel, J. A., Response surface: Design and analysis, New York: Marcel Dekker, Inc. (1987)
7. Giry, K., Viana, M., Genty, M., Wu, thrich P., Chulia, D., Surface responses and desirability functions to determine optimal granulation domains, *Drug. Dev. Ind. Pharm.*, **36**, 1016–1026 (2010)
8. Huang, Y.B., Tasai, Y. H., Yang, W. C., Chang, J. S., Wu, P.C., Optimization of sustained-release propranolol dosage form using factorial design and response surface methodology, *Biol. Pharm. Bull.*, **27**. 1626–1629 (2004)
9. Takayama, K., Nambu, N., Nagai, T.. Computer optimization of formulation of flufenamic acid/ polyvinylpolypyrrolidone/methyl cellulose solid dispersions, *Chem. Pharm. Bull.*, **31**. 4496–4507 (1983)
10. Takayama, K., Nagai, T., Simultaneous optimization for several characteristics concerning percutaneous absorp- tion and skin damage of ketoprofen hydrogels containing D-limonene, *Int. J. Pharm.*, **74**, 115–126 (1991)
11. Takayama, K., Morva, A., Fujikawa, M., Hattori, Y., Obata, Y., Nagai, T., Formula optimization of theophylline controlled-release tablet based on artificial neural networks, *J. Control Release*, **68**, 175–186 (2000)

12. Wu, P. C., Obata, Y., Fujikawa, M., Li. C. J., Higashiyama, K., Takayama, K., Simultaneous optimization based on ar- tificial neural networks in ketoprofen hydrogel formula containing O-ethyl-3-butylcyclohexanol as percutaneous absorption enhancer, *J. Pharm. Sci.*, **90**, 1004–1014 (2001)

13. Sandwell, D. T., Biharmonic spline interpolation of GEOS- 3 and Seasat altimeter data, *Geophys. Res. Lett.*, **14**, 139–142 (1987)

14. Onuki, Y., Hoshi, M., Okabe, H., Fujikawa, M., Morishita, M., Takayama, K., Formulation optimization of photocrosslinked polyacrylic acid modified with 2-hydroxyethyl methacrylate hydrogel as an adhesive for a dermatological patch, *J. Control. Rel.*, **108**, 331–340 (2005).

15. Nishikawa, M., Onuki, Y., Isowa, K., Takayama, K., Formulation optimization of an indomethacin-containing photocrosslinked polyacrylic acid hydrogel as an anti-inflammatory patch, *AAPS PharmSciTech*, **9**,: 1038–1045 (2008)

16. Obata, Y., Ashitaka, Y., Kikuchi, S., Isowa, K., Takayama, K., A statistical approach to the development of a transdermal delivery system for ondansetron. *Int. J. Pharm*. **399**, 87–93 (2010)

17. Onuki, Y., Morishita, M., Takayama, K., Formulation optimization of water-in-oil-water multiple emulsion for intestinal insulin delivery. *J Control Release*, **97**, 91–99 (2004)

18. Onuki, Y., Hoshi, M., Okabe, H., Fujikawa, M., Morishita, M., Takayama, K., Formulation optimization of photocrosslinked polyacrylic acid modified with 2-hydroxyethyl methacrylate hydrogel as an adhesive for a dermatological patch, *J. Control Release*, 108:331–340 (2005)

19. Vasconcelos, T., Sarmento, B., Costa, P., Solid dispersions as strategy to improve oral bioavailability of poor water soluble drugs. *Drug Discov. Today*, **23–24**, 1068–1075 (2007)

20. Yoshioka, M., Hancock, B.C., Zografi, G., 1995. Inhibition of indomethacin crystallization in poly(vinylpyrrolidone) coprecipitate. J. Pharm. Sci. 84, 983–986.

21. Matsumoto, T., Zografi, G., Physical properties of solid molecular dispersions of indomethacin with poly(vinylpyrrolidone) and poly(vinylpyrrolidone-co-vinyl-acetate) in relation to indomethacin crystallization. *Pharm. Res*., **16**, 1722–1728 (1999)

22. Berggren, J., Alderborn, G., Long-term stabilization potential of poly(vinylpyrrolidone) for amorphous lactose in spray-dried composites. *Eur. J. Pharm. Sci.*, **21**, 209–215 (2004)

23. Tobyn, M., Brown, J., Dennis, A.B., Fakes, M., Gao, Q., Gamble, J., Khimyak, Y.Z., McGeorge, G., Patel, C., Sinclair, W., Timmins, P., Yin, S., Amorphous drug–PVP dispersions: Application of theoretical, thermal and spectroscopic analytical techniques to the study of a molecule with intermolecular bonds in both the crystalline and pure amorphous state. *J. Pharm. Sci.*, **98**, 3456–3468 (2009)

24. Serajuddin, A. T. M., Solid dispersion of poorly water-soluble drugs: early promises, subsequent problems, and recent breakthroughs. *J. Pharm. Sci.*, **88**, 1058–1066. (1999)

25. Gregory, F. C., A Bayesian method for the induction of probabilistic networks from data. *Mach. Learn.*, **9**, 309–347 (1992)

26. Jansen, R., Yu, H., Greenbaum, D., Kluger, Y., Krogan, N. J., Chung, S., Emili, A., Snyder, M., Greenblatt, J. F., Gerstein, M., A Bayesian networks approach for predicting protein–protein interactions from genomic data, *Science*, **302**, 449–453 (2003)

27. Xue, Y., Chen, H., Jin, C., Sun, Z., Yao, X., NBA-Palm: prediction of palmitoylation site implemented in naïve Bayes algorithm, *BMC Bioinformatics*, **7**, 458 (2006)

28. Willson, W. I., Peng, Y., Augsburger, L. L., Comparison of statistical analysis and Bayesian networks in the evaluation of dissolution performance of BCS class II model drugs, *J. Pharm. Sci.* **53**, 2764–2776 (2005)

29. Kikuchi, S., Onuki, Y., Yasuda, A., Hayashi, Y., Takayam, K., Latent structure analysis in pharmaceutical formulation using Kohonen's self-organizing map and a Bayesian network, *J. Pharm. Sci.*, **100**, 964–975 (2011)

30. Cooper, E. G., Herskovitz, E., A Bayesian method for the induction of probabilistic networks from data, *Mach. Learn.*, **9**, 309–347 (1992)

31. Moore, J. W., Flanner, H. H., Mathematical comparison of curves with an emphasis on in-vitro dissolution profiles, *Pharm. Technol.*, **20**, 64–74 (1996)

32. Watanabe, Y., Koizumi, K., Zama, Y., Kiriyama, M., Matsumoto, Y., Matsumoto, M., New compressed tablet rapidly disintegrating in saliva in the mouth using crystalline cellulose, *Bio. Pharm. Bull.*, **18**, 1308–1310 (1995)

33. Bi, Y., Sunada, H., Yonezawa, Y., Danjo, K., Otsuka, A., Ikeda, K., Preparation and evaluation of a compressed tablet rapidly disintegrating in the oral cavity, *Chem. Pharm. Bull.*, **44**, 2121–2127 (1996)

34. Motomura, Y., Predictive modeling of everyday behavior from large-scale data. Synthesiology, **2**, 1–12 (2009)

35. Ulrich, B., Stewart, E. M., Gavin, N. C., Kenny. M. G., Stefan, S., Bayesian probabilistic network modeling of remifentanil and propofol interaction on wakeup time after closed-loop controlled anesthesia, *J. Clin. Monit. Comuput.*, **17**, 31–36 (2002)

36. Huang, J., Kaul, G., Cai, CS., Chatlapalli, R., Hernendez-Abad, P., Ghosh, K., Nagi, A., Quality by design case study: An in- tegrated multivariate approach to drug product and process development, *Int. J. Pharm.*, **382**, 23–32 (2009)

37. Arai, H., Suzuki, T., Kaseda, C., Ohyama, K., Takayama, K., Bootstrap re-sampling technique to evaluate the optimal for- mulation of theophylline tablets predicted by non-linear response surface method incorporating multivariate spline interpolation, *Chem. Pharm. Bull.*, **55**, 586–593 (2007)

38. Arai, H., Suzuki, T., Kaseda, C., Takayama, K., Effect of an experimental design for evaluating the nonlinear optimal for- mulation of theophylline tablets using a bootstrap resampling technique, *Chem. Pharm. Bull.*, **57**, 572–579 (2009)

39. Onuki, Y., Ohyama, K., Kaseda, C., Arai, H., Suzuki, T., Takayama, K., Evaluation of the reliability of nonlinear optimal solutions in pharmaceuticals using a bootstrap resampling technique in combination with Kohonen's seld-organizing maps, *J. Pharm. Sci.*, **97**, 331-339 (2008)

40. Hirata, M., Takayama, K., Nagai, T., Formulation optimization of sustained-release tablet of chlorpheniramine maleate by means of extreme vertices design and simultaneous optimization technique, *Chem. Pharm. Bull.*, **40**, 741–746 (1992)

41. Onuki, Y., Kikuchi, S., Yasuda, A., Takayama, K., 2010. Role of individual test samples in optimal solutions in pharmaceuticals predicted using a nonlinear response surface method, *Int. J. Pharm.*, **396**, 75–82 (2010)

42. Kikuchi, S., Takayama, K., Reliability assessment for the optimal formulations of pharmaceutical products predicted by a nonlinear response surface method, *Int. J. Pharm.*, **374**, 5–11 (2009)

43. Higgins, J. J., An introduction to modern nonparametric statistics. *Boston: Duxbury Press*. (2003)

44. Nourissat, A., Bairati, I., Samson, E., Fortin, A., Gelinas, M., Nabid, A., Brochet, F., Tetu, B., Meyer, F., Predictors of weight loss during radiotherapy in patients with stage I or II head and neck cancer, *Cancer*, **116**, 2275–2283 (2010)

45. Tang, N. S., Li, H. Q., Tang, M. L., A comparison of methods for the construction of confidence interval for relative risk in stratified matched-pair designs, *Stat. Med.*, **29**, 46–62 (2010)

46. Fahmy, R., Kona, R., Dandu, R., Xie, W., Claycamp, G., Hoag, S. W., Quality by design I: Application of failure mode effect analysis (FMEA) and Plackett–Burman design of experiments in the identification of "main factors" in the formulation and process design space for roller-compacted ciprofloxacin hydrochloride immediate- release tablets, *AAPS PharmSciTech*, **13**, 1243–1254 (2012)

47. Norioka, T., Hayashi, Y., Onuki, Y., Andou, H., Tsunashima, D., Yamashita, K., Takayama, K., A Novel Approach to Establishing the Design Space for the Oral Formulation Manufacturing Process, *Chem. Pharm. Bull.*, **61**, 39–49 (2013)

48. Watanabe, A., Hanada, T., Sugihara, M., New oral dosage form for the elderly—rapid dissolving tablet in mouth without addition of water. Yakuzaigaku, **54**, 103–110 (1998)

49. Sunada, H., Bi, Y., Preparation, evaluation and optimization of rapidly disintegrating tablets. Powder Technol. **122**, 188–198 (2002)

50. Kuno, Y., Kojima, M., Ando, S., Nakagami, H., Evaluation of rapidly disintegrating tablets manufactured by phase transition of sugar alcohols, *J. Control Release*, **105**,16–22 (2005)

51. Suda, M., Takayama, K., Otsuka, M., An accurate Quantitative analysis of Polymorphic Content by Chemometric X-ray Powder Diffraction, *Anal. Sci.*, **24**, 451–457 (2008).

52. Yoshinari, T., Forbes, R. T., York, P., Kawashima, Y., Moisture induced polymorphic transition of mannitol and its morphological transformation., *Int. J. Pharm.*, **247**, 69–77 (2002)

53. Yoshinari, T., Forbes, R. T., York, P., Kawashima, Y., The improved compaction properties of mannitol after a moisture-induced polymorphic transition, *Int. J. Pharm.*, **258**, 121–131 (2003)

54. Yamashita F., Itoh T., Yoshida S., Haidar M. K., Hashida M., A novel multi-dimensional visualization technique for understanding the design parameters of drug formulations, *Comput. Chem. Eng.*, **34**, 1306–1311 (2010)

55. Motomura Y., Predictive modeling of everyday behavior from large-scale data. *Synthesiology*, **2**, 1–11 (2009)

56. Bothtner, U., Milne, S. E., Kenny, G. N., Georgieff, M., Schraag, S., Bayesian probabilistic network modeling of remifentanil and propofol interaction on wakeup time after closed- loop controlled anesthesia, *J. Clin. Monit. Comput.*, **17**, 31–36 (2002).

57. Cunningham, J. C., Sinka, I. C., Zavaliangos, A. J., Analysis of tablet compaction. I. Characterization of mechanical behavior of powder and powder/tooling friction, *J. Pharm. Sci.*, **93**, 2022–2039 (2004)

58. Michrafy A, Diarra H, Dodds JA, Michrafy M, Penazzi L. Analysis of strain stress state in roller compaction process, *Powder Technol.*, **208**, 417–422 (2011)

59. Aydin, I., Briscoe, B. J., Sanliturk, K. Y., The internal form of compacted ceramic components: A comparison of a finite element modelling with experiment, *Powder Technol.*, **89**, 239–254 (1996)

60. Aydin, I., Briscoe, B. J., Ozkan, N., Modeling of powder compaction: A review, *MRS Bull*, **22**, 45–51 (1997)

61. Coube, O., Riedel, H., Numerical simulation of metal powder die compaction with special consideration of cracking, *Powder Metall.,* **43**, 123–131 (2000)

62. Sinka, I. C., Cunningham, J. C., Zavaliangos, A., The effect of wall friction in the compaction of pharmaceutical tablets with curved faces: A validation study of the Drucker–Prager cap model, *Powder Technol.*, **133**, 33–43 (2003)

63. Michrafy, D., Ringenbacher, D., Tchoreloff, P., Modelling the com- paction behaviour of powders: Application to pharmaceutical powders, *Powder Technol.*, **127**, 257–266 (2002)

64. DiMaggio, F. L., Sandler, I., Material model for granular soils, *ASCE J. Eng. Mech. Div.*, **97**, 935–950 (1971)

65. Häggblad, H. A., Constitutive model for powder materials, *Powder Technol.*, **67**, 127–137 (1991)

66. Jenike, A. W., Carson, J., Measurement principles of the flowa- bility of powders, *Adv. Ceram.*, **21**, 759–766 (1985)

67. Guerin, E., Tchoreloff, P., Leclerc, B., Tanguy, D., Deleuil, M., Couarraze, G., Rheological characterization of pharmaceutical powders using tap testing, shear cell and mercury porosimeter, *Int. J. Pharm.*, **189**, 91–103 (1999)

68. Han, L. H., Elliott, J. A., Bentham, A. C., Mills, A., Amidon, G. E., Hancock, B. C., A modified Drucker–Prager cap model for die compaction simulation of pharmaceutical powders, *Int. J. Solids Struct.*, **45,** 3088– 3106 (2008)

69. Wu, C. Y., Ruddy, O. M., Bentham, A. C., Hancock, B. C., Best, S. M., Elliott, J.A., Modelling the mechanical behaviour of pharmaceutical powders during compaction, *Powder Technol.*, **152**, 107–117 (2005)
70. Wu, C. Y., Hancock, B. C., Mills, A., Bentham, A. C., Best, S. M., Elliott, J. A., Numerical and experimental investigation of capping mechanisms during pharmaceutical tablet compaction, *Powder Technol.*, 181, 121–129 (2008)
71. Eiliazadeh, B., Briscoe, B. J., Pitt, K., Investigating density dis- tributions for tablets of different geometry during the compaction of pharmaceuticals, *Part. Sci. Technol.*, **21**, 303–316 (2003)
72. Peter, L. R., Ruth, C. E., A small-angle X-ray scattering study of local variations within powder compacts, *Powder Technol.*, **192**, 287– 297 (2009)
73. Djemai A, Sinka IC. NMR imaging of density distributions in tablets. Int J Pharm 319:55–62 (2006)
74. Sinka, I. C., Modelling powder compaction, *KONA*, 25, 4–22 (2007)
75. Fossum, A. F., Fredrich, J. T., Cap plasticity models and compactive and dilatant pre-failure deformation, *Proceedings of the fourth North American Rock Mechanics Symposium, Seattle, Washington*, 1169–1176 (2000)
76. Tsukamoto, T., Chen, C. Y., Okamoto, H., Danjo, K., The effects of adsorbed water on tensile strength and Young's modulus of moldings determined by means of a three-point bending method, *Chem. Pharm. Bull.*, **48**, 769–773 (2000)